University of Szeged

Faculty of Pharmacy

Institute of Pharmaceutical Analysis

MOLECULAR MIMICRY OF CONFORMATIONALLY DIVERSE β-SHEETS BY USING α/β-PEPTIDE FOLDAMERS

Ph. D. Thesis

Zsófia Hegedüs

Supervisor:

Prof. Dr. Tamás Martinek

2016

Table of Contents

List of publications and lectures

Full papers related to the thesis

I. Hegedüs, Z., Wéber, E., Kriston-Pál, É., Makra, I., Czibula, Á., Monostori, É., & Martinek, T. A. (2013). Foldameric α/β-peptide analogs of the β-sheet-forming antiangiogenic anginex: structure and bioactivity. *Journal of the American Chemical Society*, **135** (44), 16578-16584.
IF: 11.444

II. Hegedüs, Z., Wéber, E., Végh, L., Váczi, B., Tubak, V., Kriston-Pál, É., & Martinek, T. A. (2015). Two-stage interaction of the tumor nursing galectin-1 with the antiangiogenic peptide anginex. *Journal of Thermal Analysis and Calorimetry*, **120** (1), 449-456.
IF: 2.042

III. Hegedüs, Z., Makra, I., Imre, N., Hetényi, A., Mándity, I. M., Monostori, É., & Martinek, T. A. (2016). Foldameric probes for membrane interactions by induced β-sheet folding. *Chemical Communications*, **52** (9), 1891-1894.
IF: 6.567*

Other full papers

I. Németh, L. J., Hegedüs, Z., & Martinek, T. A. (2014). Predicting Order and Disorder for β-peptide Foldamers in Water. *Journal of chemical information and modeling*, **54** (10), 2776-2783.
IF: 3.738

*The impact factors for the year 2015 are given.

Scientific lectures related to the thesis

1. Hegedüs Zs., Wéber E., Kriston-Pál É., Makra I., Czibula Á., Monostori É., Martinek T. A.
   Antiangiogén foldamer β-szendvics analógok, szerkezet és bioaktivitás
   XXXVI. Kémiai Előadói Napok
   Szeged, 2013. Október 28 - 30

2. Zs. Hegedüs, E. Wéber, É. Kriston-Pál, I. Makra, É. Monostori, T. A. Martinek
   β-sandwich forming propensity and biological activity of foldameric anginex analogs
   Poster presentation
   2013 Symposium on Foldamers, Paris, 12. April 2013

3. Hegedüs Zs., Wéber E., Makra I., Czibula Á., Monostori É., Martinek T. A.
   β-redős foldamerek tervezése az angiogenezis gátló anginex analógiájára, szerkezetvizsgálat
   MTA Peptidkémiai Munkabizottság Tudományos Ülése
   Balatonszemes, 2014. május 28-30.

4. Zs. Hegedüs, E. Wéber, I. Makra, É. Monostori, T. A. Martinek
   Redesigning an antiangiogenic β-sheet peptide anginex to α/β peptide foldamers
   Poster presentation
   7th Central Europe Conference, Chemistry Towards Biology
   Katowice, 12. September 2014

5. Zs. Hegedüs, E. Wéber, I. Makra, É. Monostori, T. A. Martinek
   Membrán kölcsönhatások vizsgálata foldamerekkel, a béta redő képző hajlamuk függvényében
   MTA Peptidkémiai Munkabizottság Tudományos Ülése
   Balatonszemes, 2015. május 20-22.

Other lectures

1. Zs. Hegedüs, E. Wéber, É. Monostori, T. A. Martinek
   Interaction of foldamers with the tumor nursing protein galectin-1
   Poster presentation
   FOLDAMERS: from design to protein recognition
   Bordeaux, France, 25-28 January 2010.

Abbreviations

ACN: acetonitrile

anx: anginex

anxG: anginex-Gly

1D: one-dimensional

2D: two-dimensional

1*R*,2*S*-ACHC: 1R,2S-2-aminocyclohexanecarboxylic acid

BCA: bicinchonic acid

Bcl-2: B-cell lymphoma-2

β^3hIle: β^3-(*R*)-homoisoleucine

β^3hLeu: β^3-(*S*)-homoleucine

β^3hVal: β^3-(*R*)-homovaline

BME: β-mercaptoethanol

BSA: bovine serum albumin

CCA: convex constrain algorithm

CD: circular dichroism

CCG: Chemical computing group

DPC: dodecylphosphocholine

DOPC: dioleylphoshatidil-choline

DOPG: dioleylphosphatidil-glicine

DOSY: diffusion ordered spectroscopy

DMSO: dimethyl sulfoxide

DSS: 4,4-dimethyl-4-silapentane-1-sulfonic acid

EC: endothelial cell

EDTA: ethylenediaminetetraacetic acid

ESI-MS: Electrospray ionization Mass spectrometry

FACS: fluorescence-activated cell sorting

Gal-1: Galectin-1

Gro-a: growth related protein

HATU: 1-[Bis(dimethylamino)methylene]-1H-1,2,3-triazolo[4,5-b]pyridinium 3-oxid hexafluorophosphate

hDM2: human oncogene product double minute 2

HSQC: Heteronuclear Single Quantum Coherence

HUVEC: Human umbilical vascular endothelial cell

IC_{50} : half maximal inhibitory concentration

IL-8: interleukin-8

ITC: isothermal titration calorimetry

i.v.: intravenous

LDH: lactat dehydrogenase

MW: molecular weight

MOE: Molecular Operating Environment

NMR: nuclear magnetic resonance

NOE: nuclear Overhauser effect

NOESY: Nuclear Overhauser Effect Spectroscopy

PF-4: platelet factor 4

PFGSE: Pulsed field-gradient spin echo

PPI: protein-protein interaction

PMSF: phenylmethylsulfonyl fluoride

RP-HPLC: Reveresed phase high performance liquid chromatography

SPR: surface plasmon resonance

TFA: trifluoracetic-acid

TOCSY: Total Correlation Spectroscopy

VEC: vascular endothelial factor

wt: wild type

1. Introduction and aims

β-Sheet secondary structures are frequent among protein-protein interactions[1] (PPIs) and also present among membrane interacting peptides.[2] From a pharmaceutical point of view, these interfaces are usually undruggable by small molecule compounds because of solvent exposed surface and complex binding mechanism. The need for alternative solutions that target these interactions is reflected by the increasing number of biotherapeutics, but their application may be limited by poor pharmacokinetics, stability and immunogenicity. Non-natural β-sheet mimetic structures may overcome these disadvantages, but the construction of artificial β-sheets is an enduring challenge. The use of β-sheets as therapeutics is further hindered by their high aggregation propensity, which may result in toxic compounds.

With the help of non-natural self-organizing polymers (foldamers) both the β-sheet design and advantageous properties may be achieved. β-Peptide foldamers were successfully applied in molecular recognition processes targeting proteins and membranes, but these results were achieved mainly by using helical secondary structures.[3-5] The mimicry of β-sheets therefore requires further investigations, only a few sheet-like structures are known with biological activity.[6-12]

Our goal was to establish design strategies for conformationally diverse β-sheet folding systems by using α/β-peptide foldamers based on a selected peptide participating in protein-protein and membrane interactions. The antiangiogenic and antimicrobial peptide anginex was chosen as a model system,[13-15] which exhibits diverse structural features. It has random coil conformation in solution, and the bioactive β-sheet is formed only during interaction with the target membrane. Anginex exerts biological activity through interaction with cell membrane[16] and with the tumor nursing galectin-1 (gal-1), a β-sandwich protein, which was identified as its main target protein.[17]

Our design strategy for the α/β-peptide foldameric analogs relied on a top-down approach, systematic amino acid substitutions were made in the β-sheet region of the anginex. The folding behavior of the analogs was investigated from similar aspects that were established for the *de novo* designed β-sheets[18-24] considering also the previously determined effects of β-amino acid substitutions in hairpin systems.[25-27] After synthesis, the structural features were characterized by nuclear magnetic resonance (NMR) spectroscopy and circular dichroism (CD) techniques, which allowed the description of the local conformational preferences and overall folding tendencies of the analogs and the observation of favorable substitutions and destructuring

effects. In order to investigate their participation in PPIs, the binding to the target protein of anginex (gal-1) was investigated and characterized by isothermal titration calorimetry (ITC). Biological activity of the analogs was investigated using in vitro assays and membrane leakage experiments in cooperation with the Monostori Group in the Biological Research Centre; these experiments are part of Ildikó Makra's PhD thesis. In the present work, I would like to focus on the structural investigation and β-sheet folding behavior of these mixed α/β-foldameric structures and provide only supplementary information regarding bioactivity.

2. Literature background

2.1. β-peptide foldamers

Self-organizing non-natural folding oligomers (foldamers) are attractive tools for the construction of pre-shaped interaction surfaces for molecular recognition processes.[28] The desired orientation of pharmacophore anchor points can be controlled at the monomeric level in order to target membrane or biomacromolecules such as DNA or proteins. Among aliphatic foldamers, β-peptides that are homologs of the natural α-peptides, gained high interest in medicinal chemistry applications.[3-5]

β-Peptides are promising alternatives for natural peptides or biopharmaceuticals, because they are able to display well-folded structures using short sequences, and the placement of functional groups can be controlled. In comparison with a 150 kDa therapeutic antibody, these foldamers can exhibit folded structure and similar interaction surface even at a size of 3-5 kDa. This also lowers the chance for immune reactions, which may provide an escape from immune system; it has been shown that immune receptors that recognize α-peptides do not necessarily cross-react with α/β-peptide analogs.[29] Furthermore, proteolytic enzymes cannot recognize β-peptides [30-31] and the replacement of around 30% of the residues to β-amino acids in a peptidic sequence dramatically increases the stability against proteases.[32-34] Pharmacokinetic studies revealed elimination half-lives of 3-10 h which is significantly longer than that of an α-peptidic sequence.[35-36]

2.1.1. Building blocks and structure engineering

β-Amino acids are homologous to the natural α-amino acids and have an extended backbone chain by one methylene group, thereby they contain an additional substitution position, a possible stereogenic center and dihedral angle (Figure 1a). The major types of building blocks include open-chain amino acids with proteogenic side-chains and non-natural cyclic amino acids. β^2- And β^3-amino acids are homologs of the natural α amino acids with proteogenic side-chain on the α or β carbon atom respectively, and the synthesis of these building blocks are generally straightforward.[37] The other type of building blocks contains C^α and C^β atoms in a cycloalkane or a heterocyclic ring, which restrains their conformational space (Figure 1a). These building blocks can be utilized to stabilize a given secondary structure and preorganize the preferred dihedral constraints.[38] Peptidic foldamers can be based exclusively

on unnatural building blocks (β-peptides), and they can be prepared as mixed oligomers of α– and β-amino acids designated as α/β-foldamers.[4, 39-40]

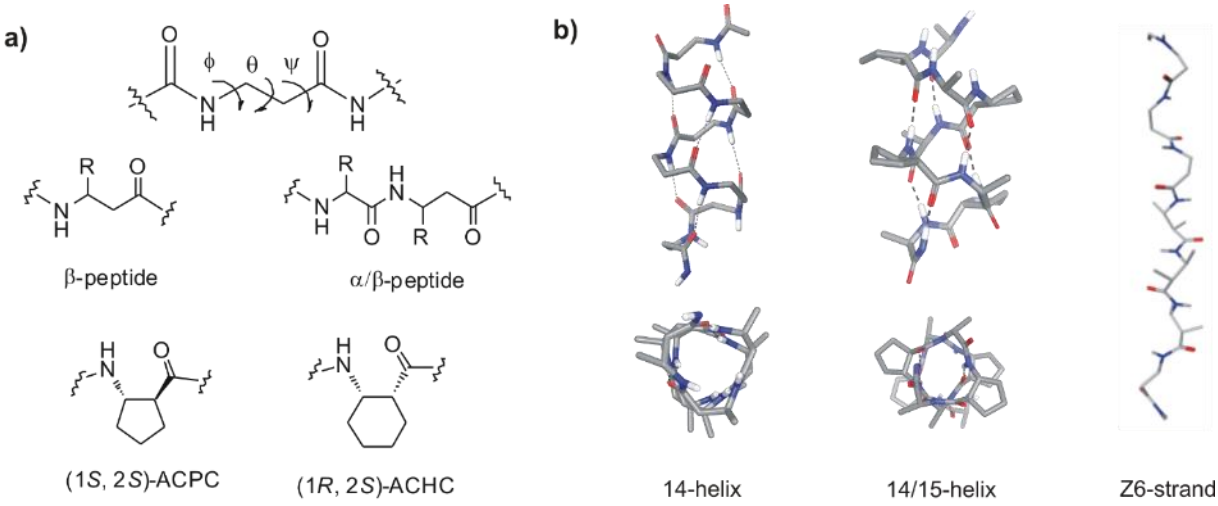

Figure 1. **a)** Definition of torsion angles for β-amino acids and examples for different building blocks and backbone structures used for peptidic foldamers. **b)** Examples for different β-peptide foldamer secondary structures.

β-Peptide secondary structures are stabilized by hydrogen-bonds, and the folding depends on local conformational preferences and long-range interactions. The structural investigation of β-peptides comprising homogeneous β- or heterogeneous α/β-amino acids led to the discovery of several turns, strands and helices (Figure 1b).[41] Foldamers comprising exclusively β^3-amino acids have been shown to form 14-helix structure.[42] The formation of 12-, 10- 8-, 18-, 10/12- and 18/20-helices were determined experimentally for pure β-peptides [41, 43-44] and α/β-peptides with heterogeneous backbone can exhibit more diverse structures.[39-40, 45] Strand-like structures were also described experimentally, which were prone to fibril formation.[46-47] A few examples demonstrate the suitability of foldamers to achieve higher ordered structures, such as helix bundles[48] or mimicry of tertiary structures.[49]

The rational design of secondary structures can be achieved through a methodology regarded as "stereochemical patterning" approach.[50-52] The desired secondary structure formation can be determined at the monomeric level by the conformation and stereochemistry of the used β-amino acid units. If the signs of the torsion angles flanking the amide bond (ϕ and ψ) are the same, then a helical structure is induced if they are opposite, then strand formation is preferred. The signs of the dihedrals determine also the amide-bond orientation.

To engineer function, two general design approaches have been used most commonly for foldamers: structure-based or sequence-based design strategies. Structure-based approach requires the knowledge of the appropriate presentation of hot spot or epitope residues derived

from the preferred conformation of a macromolecule.[53] The goal is to choose an appropriate scaffold and functionalize it with proteogenic side-chains that are able to mimic the position of the epitope residues. With this approach the entire geometrical arrangement of the original structure cannot be mimicked but the similar presentation of functional groups may mimic its binding properties. The advantage of this approach is that the side-chain functionality is assumed not to affect the secondary structure of the scaffold, therefore it enables the testing of different side-chain functionality, regardless of the secondary structure.

Sequence-based design is an alternative strategy, which relies on the optimization of a scaffold structure.[26, 54] This approach requires the knowledge of a peptidic sequence or partial sequence that interacts with the target, and the substitution of its residues with β-amino acids.[4] The optimization is carried out on the backbone structure, while the side-chain functionality generally remains constant. This approach results in foldamers with heterogeneous backbones, which can be further optimized and stabilized to achieve the appropriate fit to the target.

In case of more complex interaction interfaces alanine-scan or β-amino acid scan of a known sequence can aid the selection of residue positions which are available for non-natural amino acid substitutions.[32] Additional approaches, such as fragment- [55] or library-based[56-57] methods, could also be utilized but these did not gain frequent application among foldamers.

2.1.2. Mimicry of protein structure and function

The ability of foldamers to fold to well-defined secondary structures with appropriate positioning of the proteogenic side-chains makes them excellent tools for mimicry of protein interaction surfaces. Table 1 summarizes the foldameric designs with potential biological activity targeting proteins.

Table 1. Summary of peptidic foldamers targeting protein-protein interactions

Target	Design principle	Structure	Reference
hDM2	Mimicry of hot-spot residues of p53 activation domain	14-helix	58, 59, 60
Bcl-2 /Mcl-1	Structure-based mimicry of BAK BH3 domain	chimera α+α/β helix	61, 62
	Sequence-based strategy based on PUMA BH3 domain	helical ααβαααβ substitution pattern	63
	Sequence-based strategy based on Bim BH3 domain	helical ααβαααβ and αααβ substitution patterns	63
$\alpha_{IIb}\beta_3$ domain of integrin	Mimicry of CHAMP peptides	12-helix	64
γ-Secretase	Highly hydrophobic helical structure design	12-helix	65, 66
HIV fusion protein, gp41	Structure-based mimicry of WWI epitope	14-helix	67, 68
	Sequence-based substitution strategy based on the CHR domain of gp41	helical, ααβαααβ substitution pattern	69, 70
beta Amyloid	Fragment-based approach targeting the repeating sequence of the protein	14-helix	55
VEGF receptor	Substitutions in an optimized VEGF binding peptide v114	unstructured	71
VEGF, IgG, TNF-α	Sequence-based optimization of the Z-domain scaffolds	diverse, helical	72
PTH receptor	Sequence-based optimization of PTH_{1-34}	helical, αααβ substitution pattern	73
Glucagone receptor	Sequence-based optimization of GLP-1	helical, αααβ substitution pattern	74

hDM2: human double minute 2; Bcl-2: B-cell lymphoma 2; Mcl-1: Myeloid cell leukemia 1; PUMA: p53 upregulated modulator of apoptosis; BAK: Bcl-2 homologous antagonist killer; BH3: Bcl-2 homology domain 3; CHAMP: computed helical anti-membrane protein; CHR: C terminal heptad repeat; VEGF: vascular endothelial growth factor; PTH: parathormon; GLP-1: Glucagone-like protein-1

Mimicking helices by foldamers

A number of PPIs are mediated by isolated α-helical secondary structures.[75] These interfaces are frequently targeted with foldamers, because the design strategies for foldameric helices or structural mimetics are well established. A number of non-natural scaffolds are available that are able to mimic a helical structure that recognize a binding cleft on the target protein.

Most of the structure-based approaches utilized the 14-helical scaffold to present functional side-chains (Figure 2a). Two faces of the helix are responsible for structural stability, which can be enhanced by ion-pairing interactions on one side of the helix to achieve good stability and solubility in water.[76] The proteogenic side-chains can be placed in order to point toward the interaction surface. With this design strategy effective inhibitors were constructed to block interaction of p53 and the human oncogene product double minute 2 (hDM2)[58-60] protein which may lead to p53 mediated apoptosis in certain tumor types and tumor regression. Furthermore the epitope residues of gp41 HIV fusion protein were effectively mimicked with this strategy which may lead to block the HIV entry to cells.[67-68]

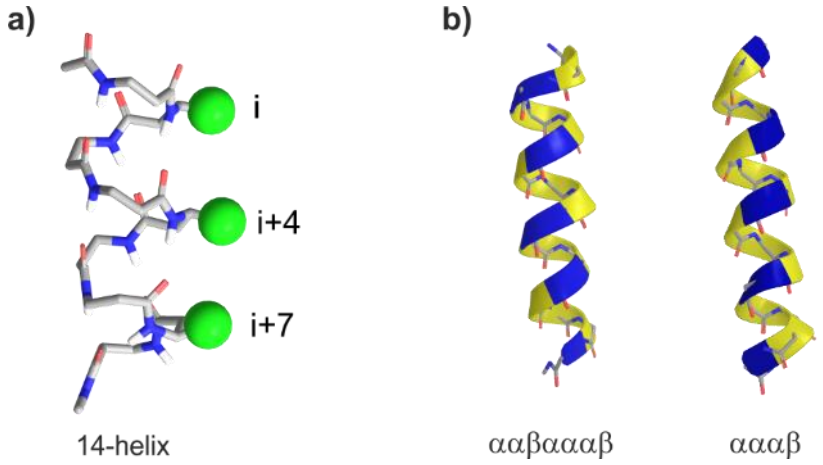

Figure 2. Common design strategies for bioactive foldameric helices. **a)** Mimicking side-chain orientation in positions i, i+4 and i+7 by using a 14-helical scaffold, epitope residues are highlighted green. **b)** Common substitution patterns utilized during top-down helix design approaches, β-amino acid residues are highlighted blue.

The choice of the substitution patterns in sequence-based helix mimetic structures often relies on the heptad repeat motif of the α-helix in ααβαααβ backbone pattern, which results in a β-amino acid stripe created along one side of the helix (Figure 2b). This face of the helix is generally kept away from the interaction interface, however, it was shown that the isolation of β-amino acids are not necessary and tuning of selectivity can be achieved by utilizing them in interaction with the protein.[63] Along with the ααβαααβ pattern other repeating units such as ααβ or αααβ can adopt helical conformations (Figure 2b) and result in very similar structures to the original α-helix.[77] Constrained residues are widely used for substitutions as they enhance the helical fold and stability, which may contribute to the affinity of the ligand. These strategies were employed during the effective design of inhibitors of the anti-apoptotic Bcl-2 protein family[61-62] and HIV fusion protein[69-70] among other examples (Table 1). These successes of the

foldamers in this field highlight their ability to accommodate the structural requirements of helix-mediated PPIs.

Mimicking β-sheets by foldamers

Whereas the top-down approach to construct bioactive foldameric helices has become successful,[78] the rules of possible β-amino acid replacements in β-sheets have remained to be investigated. Structural elements such as the fibrillous β-peptidic nanostructures[47, 79-80 64], short turns[81-84], and a three stranded sheet in organic solvent[85] are described among β-peptide foldamers. Sheet-structures that were stabilized by macrocyclization and a non-peptidic template showed bioactivity[6-12] but only a few other bioactive strand or β-sheet like structures are known.[86]

The top-down approach starting from α-peptidic β-hairpins has revealed complex behavior when the β-amino acid substitutions were made in the hydrophobic core. In matching positions of the two strands, the α → β^3 modification resulted in an altered hydrogen-bond pattern and side-chain display as compared with the natural β-sheet structure (Figure 3b),[25] which led to decreased structural stability. α → β^3 Amino acid substitution with matching stereochemistry to the natural α-amino acids were tolerated, and α → *trans*-$\beta^{2,3}$ substitution resulted in an oligomer that displayed more stable fold compared to the natural hairpin. Other amino acid types, including cyclic residues, exhibited decreased folding after the substitution position or no overall folding.

Alternative design strategies with the goal of maintaining the native side-chain orientation utilized substitutions of two α-amino acid residues by a single β-amino acid (αα → β^2 or β^3), or applied special $\beta^{2,3}$-residues (Figure 3c).[26] These substitution strategies have been tested for 16-residue disulfide-cyclized β-hairpin peptides with a hydrophobic cluster of four amino acids and resulted in a native-like hairpin fold. The focus has been placed on the structural stability, but these sequence changes may lead to the loss of key side-chains in a biologically active β-sheet as a result of the replacement of two amino acids. This promising strategy using αα → β or ββ substitution was not suitable in a more complex tertiary structure and tolerated only more conservative N-methyl-α-amino acid alterations on the two terminal strands of a four-stranded β-sheet part.[27]

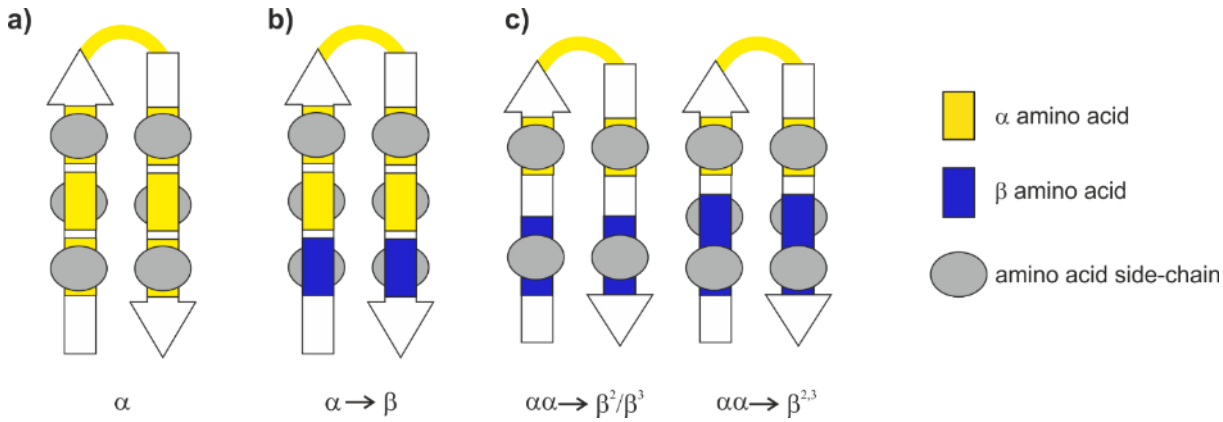

Figure 3. Different strategies for β-amino acid substitutions in hairpin systems and the caused alteration in side-chain display**. a)** Natural side-chain display of a hairpin. **b)** Single α → β substitutions that cause altered side-chain orientation in the substitution position. **c)** Double αα → β substitutions that maintain original side-chain orientation but cause loss of functionality or requires special amino acids.

It is not fully understood yet whether the core α → β mutations in a hydrophobically stabilized system cause the same alterations as in the hairpin models. In a protein-sized model system which was based on substitutions in betabellin-14 highlighted the importance of the side-chain packing interactions and the steric requirements of the substituted amino acids and 1*R*,2*S*-aminocyclohexane-carboxylic acid (1*R*,2*S*-ACHC) was shown to fit into the hydrophobic cluster of the β-sandwich structure out of a number of tested cyclic residues.[87]

2.1.3. Membrane targeting foldamers

The basic requirement for membrane interaction of a peptide is its amphiphilic character with positively charged residues, which are attracted to the negatively charged membrane components and disrupts its structure. The well-folded structure of foldamers is suitable for the separation of hydrophobic and hydrophilic residues and to construct structures with overall amphiphilic character. With these design principles antimicrobial and cell-penetrating foldamers could be constructed.[88-91] The main problem with the design of such foldamers is to distinguish between the membrane of pathogenic and eukaryotic cells, a number of foldamers however displayed low hemolytic activity.[92]

The analysis of the foldamers revealed that selectivity was dependent on the balance between hydrophobicity, charge distribution and structure. It was shown that the construction of rigid, preformed, globally amphiphilic structure is not necessary.[93] It supported that a backbone which allows the adoption of amphiphilic conformation upon membrane interaction is sufficient. Hemolytic activity was correlated with the lipophilicity of the structures, which

suggested that the hydrophilic/lipophilic balance of the peptides were important regarding selectivity.[93]

2.2.Folding behavior of *de novo* designed β-sheets

Investigation of the driving forces of folding into a β-sheet and stability was carried out through several designed small hairpin structures. They are considered as minimal model systems of β-sheet as they have two antiparallel strands linked by a short loop.[94-96] The β-sheet part of platelet factor-4 (PF4), interleukin-8 (IL-8) and growth related protein (Gro-α) aided the design of several 33-mer water soluble β-sheet peptides called the βpep series.[18-24] Another design strategy resulted in higher ordered β-sandwich structures with high propensity to aggregation.[97-100] These designs highlighted the importance of the turn segment as well as the residue composition and the stabilizing interstrand interactions and hydrophobic forces (Figure 4). These rules that have been established during the *de novo* design of minimal β-sheet model systems and the higher ordered, hydrophobically stabilized β-sheets may help us to improve the design strategies and extend to α/β-peptidic systems.

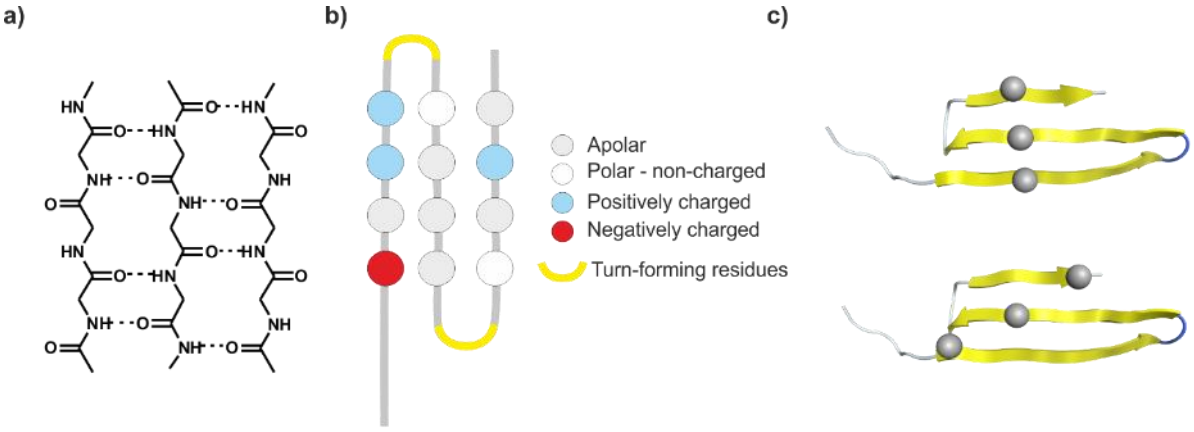

Figure 4. Design rules and basic features of *de novo* designed β-sheets. **a)** Hydrogen-bond pattern of an antiparallel β-sheet. **b)** Proper amino acid composition of the peptide. **c)** Lateral and diagonal side-chain overlap, which contributes to stabilizing hydrophobic interactions.

2.2.1. Folding initiation

During the folding of β-hairpins the turn initiation is particularly important. The loop segment of a β-hairpin contributes to the overall stability, determines the turn type and also the interstrand residue pairing pattern. The amino acid composition of the turn affects the final conformation of the β-hairpin as its early formation reduces the conformational space and allows the development of specific interactions between the strands.[101] Transient interstrand

hydrogen-bond further reduces the conformational space, which eventually leads to the typical hydrogen-bond pattern of a β-sheet (Figure 4a).[102]

2.2.2. Residue composition and solubility

In order to avoid high aggregation potency, the optimal equilibrium between water solubility and self-assembly has to be found for β-sheets. Residue composition contributes to the overall folding and solubility of the peptide. For combining peptide solubility with a high propensity of β-sheet folding, a number of rules has been established (Figure 4b).[18] Adjusting the overall net charge to positive values was found to maintain solubility, with positive to negative residue ratio between 4:2 and 6:2, which also facilitates interchain repulsion and avoiding aggregation. Polar side-chains contribute to increased solubility, but too high number of polar side-chains decreases the stabilizing hydrophobic forces and leads to decreased folding. Less than 20 % non-charged polar residues are therefore recommended. The incorporation of aliphatic residues is the most important for the development of stabilizing interactions, 40 - 50 % of the residues should contain aliphatic side-chains.

2.2.3. Hydrophobic effects

Properly aligned strand residues develop favorable interstrand side-chain interactions, therefore the composition and the location of amino acids with different properties are particularly important. The interaction between laterally paired hydrophobic side-chains has high contribution to antiparallel β-sheet stability (Figure 4c). Diagonal side-chain interactions possibly take part in β-sheet stability.[95, 103] It has been shown that the turn residues have a cooperative folding effect with the adjacent hydrophobic cluster; closer hydrophobic core to the turn increased the stability of a hairpin.[19, 104] It has been shown that Ile and Leu residues fit best to the tight packing in the β-sheet core.[18]

In contrast to helical systems, where folding cooperativity increases with longer chain length, the cooperative folding in a β-sheet system should be considered in two directions: along with the chain and perpendicular to it. Experiments showed that lengthening a β-hairpin strand from four to seven residues increased stability, however further lengthening did not result in more stable structures.[105] Increasing strand number resulted in more stable β-sheet fold, which was explained by the conformational preorganization of each strand of a β-hairpin to an additional strand.[106] It was shown that β-sheets tend to self-associate as further stabilization and form higher ordered structures such as dimers and tetramers.[107]

2.3. Anginex

In our investigations, the 33-mer three-stranded antiparallel peptide from the *de novo* designed βpep series, the βpep25 known as anginex[15] was used as a β-sheet model system.

2.3.1. Structure

Anginex belongs to the membrane-interacting peptides that exhibit diverse conformational changes upon interaction with the target[2] and exhibits concentration and target-dependent structural diversity. At low micromolar concentrations in solution, anginex displays high content of random coil conformation and exists in a monomeric form.[107] In the presence of lipid micelles even at low concentration of anginex the β-sheet folding can be induced as shown by CD measurements.[16] At higher, millimolar concentrations anginex forms tetrameric associations and exhibits high β-sheet content.[107-108] The CD curve of both synthetic and recombinant anginex showed β-sheet characteristics at 100 μM concentration.[109]

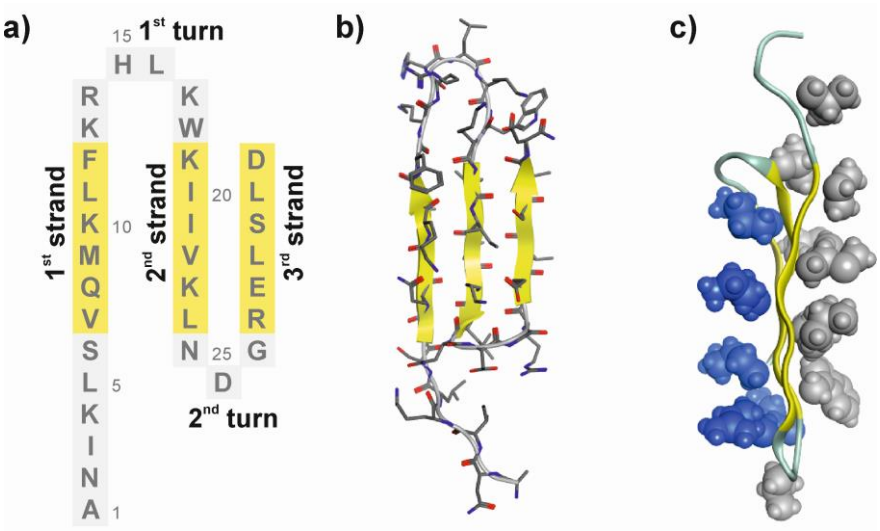

Figure 5. a) Sequence of anginex with indication of the strands and turns. **b)** Model structure of anginex based on the literature data and **c)** hydrophobic (grey) and hydrophilic (blue) residues highlighted in the model structure indicating the polar and apolar surfaces of anginex and its amphiphilic character.

High-resolution structure of anginex was obtained in the presence of dodecylphosphocholine (DPC) micelles in a solution of H_2O:DMSO 1:1.[110] Without the micelles at 500 μM peptide concentration, anginex exhibited chemical shift characteristics of a random coil conformation. Addition of DPC changed the spectral characteristics showing well dispersed and downfield shifted H^{α} and NH resonances that were related to β-sheet fold. The high-resolution structure was derived from several cross-strand NOE backbone to backbone interactions, which revealed an antiparallel β-sheet fold comprising of three strands. The strands

anginex-(7-12), -(19-24) and -(28-33) are connected by the turns [14-17] and [25-27], respectively (Figure 5a). This supersecondary structure resulted in the spatial separation of the hydrophobic and hydrophilic residues that generated an apolar and a cationic surface, respectively (Figure 5b, c).

The stability of the turn segments were different. Resonances were broad for the first turn and could not be assigned; however, the second turn showed upfield shifted resonances, which indicated a well folded tight turn. NOEs observed between strands 1 and 2 were generally weaker than between 2 and 3, and also chemical shift analysis pointed out that downfield shifted resonances indicating β-sheet formation was higher in strand 2 and 3. These data suggested a higher flexibility for the first turn.[110]

2.3.2. Biological activity

Two main biological functions were identified for anginex: antitumor[111] and antibacterial[112] activity. In the following the antitumor activity will be discussed as it was investigated for the designed foldameric analogs.

Anginex exerts its antitumor activity through angiogenesis inhibition. Angiogenesis, the formation of new capillaries, provides nutrient supply to solid tumors and facilitates tumor growth and metastasis formation. Angiogenesis inhibitors are therefore promising agents in antitumor therapy.[113-116] Anginex inhibits vascular endothelial cell (VEC) proliferation adhesion and migration, which leads to decreased angiogenesis. Anginex showed specificity toward activated endothelial cells with no toxicity to normal tissue.[14, 117] The proliferation inhibition of human endothelial cell (EC) lines were more pronounced, but regarding migration inhibition mouse ECs were more sensitive.[14] Antiangiogenic effects were proved *in vitro* and *in vivo* studies, which showed the inhibition of sprout formation and reduced vessel formation.[14, 117]

Anginex inhibited tumor growth dose-dependently in animal models, and reduced vessel formation was observed in the treated animals at a maximal dosage of 10mg/kg/day.[14, 118] Anginex alone significantly inhibits tumor growth but the combination with other antitumor therapies such as radiotherapy or conventional chemotherapy has been shown to be successful.[119-122] The combination treatment with carboplatin, radiotherapy or angiostatin exhibited a synergistic effect that resulted in effective tumor reduction or regression.[123-124] Administering anginex before radiation treatment resulted in further decrease in EC survival by direct sensitization.[125] Pharmacokinetic experiments showed fast degradation and low serum

half-life of approximately 50 min after i.v. injection, which required continuous supply by osmotic minipumps.[14]

The exact mechanism of action of anginex in not fully understood yet, for *in vivo* activity fibronectin, a plasma adhesion molecule is required which homes anginex to angiogenic blood vessels.[126]

2.3.3. Structure-activity relationships

Despite the prevailing random coil conformation at low concentrations as used in biological assays, the β-sheet was found as the bioactive conformation for the antiangiogenic effect[127], which suggested that the bioactive conformation folded only upon interaction with the target. Leu^{5}, Val^{7}, Lys^{10}, Lys^{17}, Ile^{20}, Val^{22} and Leu^{24} were found key residues in *in vitro* structure-activity studies carried out with a number of β-sheet forming analogs[13] and Ala scan derivatives.[128] Based on these observations anginex analogs were synthesized retaining only part of the peptide and mimicking the first turn with a dibenzofurane ring, which resulted in a more potent antitumor analog.[128]

2.3.4. Interaction with gal-1

A beta galactoside binding protein gal-1 was identified as a molecular target of anginex. Gal-1 is highly expressed in tumor cells and plays a role in tumor cell adhesion, migration and angiogenesis, and is a potential target for antitumor therapy.[129-131] The major secondary structure of gal-1 is also β-sheet, and folds into a β-sandwich structure that forms homodimers in solution with dimerization K_D of 1-7 μM.[132-133] Anginex treatment in gal-1 null mice did not result in tumor suppression, which highlighted the importance of gal-1 in anti-angiogenic effect of anginex.[17]

NMR investigations of gal-1 protein showed significant chemical shift changes upon interaction with anginex, however, there is no high resolution structural data available of the gal-1 anginex complex.[17] NMR data of a dibenzofurane containing analog of anginex suggested allosteric inhibition sites of gal-1.[134] The mechanism of interaction is studied mainly by solid-phase methods and mass spectrometry. Surface plasmon resonance experiment suggested that anginex dimer binds to gal-1 with biphasic dissociation pattern with K_D of 6.4 μM for the first and 90 nM for the second anginex molecule, and this stoichiometry was suggested by MS measurements also.[17] Fluorescence anisotropy measurements revealed enhanced glycoprotein binding upon interaction with anginex,[135] but the mechanism and its biological relevance is not

clear. It was speculated that the altered affinity toward glycoproteins might shift the equilibrium of gal-1 receptor binding and inhibit the reversibility of interactions that is required for its functions. The exact interaction and biological relevance of anginex-gal-1 complex is not clear yet and requires further investigations, including solution-phase characterization.

2.3.5. Interaction with membranes

Fluorescence-activated cell sorting (FACS) experiments on HUVEC cells showed dose-dependent cell fragmentation upon anginex treatment accompanied by increased LDH release and decrease in cellular ATP level.[16] Fluorescein-conjugated anginex showed localization in the membrane by confocal microscopy. These results suggested that membrane interactions are a key component in the activity of anginex.

The interaction with membrane components was further investigated by artificial phospholipid micelles that contained dioleyl-phophocholine (DOPC) dioleyl - phosphatidylserine (DOPS) or dioleyl-phophatidylglycine (DOPG) mimicking neutral and negatively charged cell membrane surfaces respectively. Anginex displayed high affinity and selectivity against the negatively charged micelles that is known to mimic cells activated by growth, stress or apoptosis by translocation of the negatively charged phospholipids after activation.[136] This selectivity is also reminiscent of membrane targeting antibacterial compounds and possibly plays a key role in the antibacterial activity of anginex.

Exact mechanism of membrane interaction is however unknown, the β-sheet formation occurs upon interaction with lipids even at lower concentrations. Solid state NMR investigations revealed unique orientation in lipid layer which is consistent with all of the general methods of membrane disruption by peptides such as pore-forming mechanism or carpet-mechanism.

3. Experimental methods

3.1. Peptide synthesis and purification

Peptide amides were synthesized by using CEM's Liberty 1 microwave peptide synthesizer. Anginex-Gly and **2c** were synthesized also by continuous flow peptide synthesis.[137] In both synthetic methods, Tentagel R RAM resin was used as solid support and 1-[bis(dimethylamino)methylene]-1*H*-1,2,3-triazolo[4,5-*b*]pyridinium 3-oxide hexafluoro-phosphate (HATU) as coupling reagent. During microwave enhanced synthesis, couplings were performed in a 3-equivalent amino acid excess at 75 °C for 15 min for α-amino acids, and for 30 min for β-residues. In order to avoid racemization, histidine was coupled at 50 °C. Arginines were coupled in two cycles. To avoid aspartimide byproduct formation between Asp^{26}-Gly^{27} and epimerization of Asp^{33}, Fmoc-Asp(OtBu)-Gly(Dmb)-OH was used in these couplings.

In the continuous flow method, Tentagel resin was filled into a HPLC column and a 1.5 equivalent amino acid excess was used for β-amino acids and Fmoc-Asp(OtBu)-Gly(Dmb)-OH couplings. Recirculation of the coupling mixture on the resin was applied for 30 min. For α-amino acids, an excess of 3 equivalents was used without recirculation. All couplings and deprotection cycles were carried out at 50 °C, 70 bar at a flow rate of 0.15 ml min^{-1}, with a 10-min washing step between the cycles.

Cleavage was performed with trifluoroacetic-acid (TFA) /water/D,L-dithiothreitol/triisopropylsilane (90:5:2.5:2.5) for 3h, which was followed by TFA evaporation and precipitation of the peptide in ice-cold diethylether. The resin was washed with acetic acid and water, then filtered, and lyophilized. Peptides were purified with RP-HPLC on a C18 column (Phenomenex Jupiter, 10 x 250 mm). HPLC eluents were: (A) 0.1% TFA in water and (B) 0.1% TFA, 80% acetonitrile (ACN) in water, with a gradient from 30% to 60% B in 60 min or 35-65% in 60 min depending on the hydrophobicity of the peptides, at a flow rate of 4 ml min^{-1}. Purity was confirmed by analytical RP-HPLC and ESI MS measurements. Peptide purity was above 95% for all compounds according to analytical RP-HPLC measurements.

3.2. Circular dichroism measurements

Samples for CD measurements were prepared in 10 mM K-phosphate buffer (pH 5.6) using 100 μM peptide concentration. For measurements with DPC, buffer was prepared with 2.5 mM DPC concentration.

CD measurements were performed with a Jasco J-815 CD-Spectrometer. CD spectra were recorded by using a thermally jacketed quartz cuvette with 1 mm optical length, from 260 to

190 nm, at a scan speed of 100 nm min^{-1} with 8 accumulations. For thermal control, a Julabo water thermostat was used with a 10 min equilibration time for each temperature. Equally measured solvent baseline was subtracted. All CD spectra were normalized to chromophoric units (residue number). All measured spectra were deconvoluted with convex consraint algorithm (CCA+) software[138-140] to three pure components.

3.3.NMR experiments

Samples for NMR measurements were prepared in a capillary NMR tube, at a concentration of 0.5 mM in 20 mM, d18-HEPES buffer (pH 5.6, 90% H_2O, 10% D_2O) containing 0.02% NaN_3. For ^{13}C Heteronuclear Single Quantum Coherence (HSQC) measurements samples were prepared in the same concentration but the buffer contained only D_2O. For measurements with DPC samples were prepared in 10 mM pH 5.6 K-phosphate buffer containing 12.5 mM DPC in order to match the conditions and peptide:lipid ratio with the CD measurements. For referencing, 4,4-dimethyl-4-silapentane-1-sulfonic acid (DSS) was used as an external standard.

NMR spectra were recorded on a Bruker Avance III 600 MHz spectrometer equipped with a 5 mm CP-TCI triple-resonance cryoprobe. For resonance assignment, 2D homonuclear Total Correlation Spectroscopy (TOCSY) and Nuclear Overhauser Effect Spectroscopy (NOESY), and 2D heteronuclear ^{13}C HSQC experiments were performed. The NOESY mixing time was 225 ms and the number of scans was 32. TOCSY measurements were made with homonuclear Hartman–Hahn transfer, using the DIPSI2 sequence for mixing, with a mixing time of 80 ms, the number of scans was 32. For all the 2D homonuclear spectra, 2K time domain points and 512 increments were applied. Signal assignment was based on the 2D NMR spectra obtained at 37 °C. 1D ^1H NMR spectra of the 0.5 mM samples were also measured with 12.5 mM d18-DPC. All ^1H spectra were acquired with the excitation sculpting solvent suppression pulse scheme.[141] Processing was carried out by using Topspin 3.1 (Bruker), a cosine-bell window function, single-zero filling, and automatic baseline correction. Spectra were analyzed by using Sparky 3.114 (T. D. Goddard and D. G. Kneller, University of California, San Francisco).

Pulsed field-gradient spin echo (PFGSE) NMR measurements. PFGSE NMR measurements were performed at 37 °C by using the stimulated echo and longitudinal eddy current delay (LED) pulse sequence with excitation sculpting for water suppression.[141] A time of 3 ms was used for the dephasing/refocusing gradient pulse length, and 300 ms for the diffusion delay. The gradient strength was changed quadratically (from 5% to 80% of the maximum value); the number of steps was 32. Each measurement was run with 64 scans and

8K time domain points. Diffusion Ordered Spectroscopy (DOSY) measurements were processed and evaluated by using the exponential fit implemented in Topspin 3.1. For processing, exponential window function and single zero filling were applied.

3.4. Production and purification of recombinant wild-type and V5D mutant human gal-1

Cloning, transformation and optimization of expression and purification conditions for the wild type and the mutant gal-1 was done by Lea Végh and Balázs Váczi in the Éva Monostori group, Biological Research Centre, Szeged. For wild-type (wt) gal-1, the huGal-1 cDNA sequence was amplified and cloned into the pET26b bacterial expression vector (forward primer: 5'CGCCATATGGCTTGTGGTCTGGTCG; reverse primer: 5'CGGGATCCTCAGTCAAAGGCCACACATTTGAT) and transformed to BL21(DE3)RIL *E. coli.* For V5D-gal-1, human wt gal-1 cDNA sequence was amplified with primer containing the V5D mutation and cloned into pET26 bacterial expression vector (forward primer: 5'GATATACATATGGCTTGTGGTCTGGACGCCAGCAAC; reverse primer: 5'CGGGATCCTCAGTCAAAGGCCACACATTTGAT) and transformed to BL21(DE3) *E. coli*.

Bacteria expressing wt or V5D gal-1 were grown in LB containing 15 μg/ml kanamycin and 10.4 μg/ml chloramphenicol or 15 μg/ml kanamycin, respectively. The expression and purification steps were identical for the two proteins. The starter pellet from 1 ml of LB culture was inoculated into 500 ml of LB medium, followed by culturing at 37 °C. When OD_{600} reached the range 0.5-0.7, expression was induced with 0.5 mM isopropyl β-D-thiogalactopyranoside, followed by overnight incubation at 18 °C. The induced culture was pelleted (4500 rpm, 17 min, 4 °C) and stored at -80 °C.

All purification steps were performed at 4 °C. The cell pellet from the 500 ml induced LB culture was resuspended in 50 ml of ice-cold lysis buffer, 50 mM Tris pH 7.5, 10 mM ethylenediaminetetraacetic acid (EDTA), 1 mM phenylmethylsulfonyl fluoride (PMSF), 4 mM β-mercaptoethanol (BME) with gentle pipetting. The cell culture was lysed with a French press. After centrifugation, the supernatant was filtered and applied to a 3 ml α-lactose agarose column. Tris buffer (50 mM Tris pH 7.5, 1 mM PMSF, 4 mM BME) was used for equilibration and washing. Bound proteins were eluted with elution buffer (30 mM β-lactose, 50 mM Tris pH 7.5, 4 mM BME) into 5 ml of 50 mM Tris pH 7.5, 4 mM BME solution to avoid precipitation due to high concentration. Fractions were collected and dialyzed for 24 h at 4 °C. The dialysis buffer (10 mM NH_4Ac pH 7.4, 4 mM BME) was exchanged at regular times: after 1 h dialysis,

1 l of buffer was replaced; then, following 3 h, overnight and another 3 h dialysis, 5 l of fresh buffer was used. This method usually yielded 7-10 mg of wt and 2-3 mg of V5D gal-1 from 500 ml of cell culture. Protein concentrations were validated with the bicinchonic acid (BCA) assay, using bovine serum albumin (BSA) for calibration.

3.5. Isothermal titration calorimetry

ITC experiments were carried out with a MicroCal VP-ITC microcalorimeter. The optimized binding experiments were performed in 20 mM Tris buffer (pH 7.4) at 35 °C. In the individual titrations, the injection volume and the spacing between titration points were adjusted, depending on the peak width and height determined in the preliminary experiments. 10-20 μl of anginex-Gly solution was injected from the computer-controlled microsyringe into the gal-1 solution at intervals of 300 - 600 s. The gal-1 concentration in the cell was 15 μM, and the concentration of anginex-Gly varied between 80 μM and 175 μM. Control experiments were performed by injecting anginex-Gly into the cell containing buffer with no target. Experimental data were fitted to the two independent sites model (adjustable parameters: ΔH_{b1}, K_{D1}, n_1 and ΔH_{b2}, K_{D2}, n_2) by using a nonlinear least-squares procedure. Fitting error was calculated using jack-knife method.[142] The stoichiometries (n_1 and n_2) are given for the monomeric gal-1 chain.

3.6.Molecular modelling

In order to generate the molecular coordinates for anginex we utilized distant restraints in Ref. 110. This procedure involved manual model construction and initial folding into the proposed β-sheet, then 10 ns molecular dynamics simulation was run with the literature NOE distance restraints. The simulations were run with Amber ff03 forcefield and implicit water model implemented in Chemical computing group's (CCG) Molecular Operating Environment (MOE). We selected the lowest energy structure from the trajectory for further evaluation and compared the overall fold with the literature result. In order to visualize the fit of the β-amino acid residue into the β-sheet geometry, a single residue was replaced and minimizations were run in two stages. First, the unchanged residues were tethered to their original positions, and second, a minimization was run without any restraint.

4. Results and Discussion

4.1. α/β-foldameric analogs of anginex

4.1.1. Sequence design

Investigation of the effects of β-amino acid substitutions has been carried out mainly in smaller hairpins[25,26], and it is not known whether α → β substitutions in a three-stranded, hydrophobically stabilized system cause the same alterations in the structural stability. The basic principles of our design strategy therefore relied on the rules established for *de novo* designed natural β-sheets[13, 18, 107], because the folding behavior of α/β-peptide mimetic structure may be more similar to its natural counterpart. Our aim was to explore the effects of β-amino acid substitutions in the β-sheet forming region of the model peptide anginex, and to investigate the folding behavior and biological activity of the α/β-analogs.

Substitution positions and patterns were designed with the goal of maintaining the original hydrogen-bond pattern and side-chain orientation of the β-sheet focusing mainly on the hydrophobic face of the peptide. The majority of the residues in the β-sheet region of anginex are important for bioactivity as was shown in *in vitro* tests.[128, 143] These involve hydrophobic side-chains responsible for stabilization and pharmacophore points over the surface of anginex. Our goal was therefore to avoid design strategies that involve amino acid deletion, such as αα → β substitutions, thus we utilized single α → β substitutions in order to maintain all possible pharmacophore points. Substitutions were designed to keep the two turn-forming regions of anginex intact to maintain appropriate turn initiation. β-Amino acid replacements were carried out in the three β-sheet forming strand segments involving anginex-(7-12) residues in the first, -(19-24) in the second and -(28-33) in the third strand (Figure 6).

β-residues may alter the peptide bond and side-chain orientations, replacements in matching positions (in-registry substitutions) are therefore expected to minimize these destructuring effects. Six such positions were available in the β-sheet region of anginex, denoted by numbers 1-6 (Figure 6). These positions involved three hydrophilic (2, 4 and 6) and three hydrophobic (1, 3 and 5) triplets. In order to highlight the effects of matching substitutions, two other positions were selected with non-matching replacements in this system: a diagonal (7) and the sequential (8) pattern.

Five different substitution patterns were designed, denoted by letters **a**-**e** (Figure 6), pattern **a** was utilized in all positions (**1**-**8a**) patterns **b**-**e** were tested only in the hydrophobic face of the peptide (**1b**-**e**, **3b**-**e**, and **5b**-**e**).

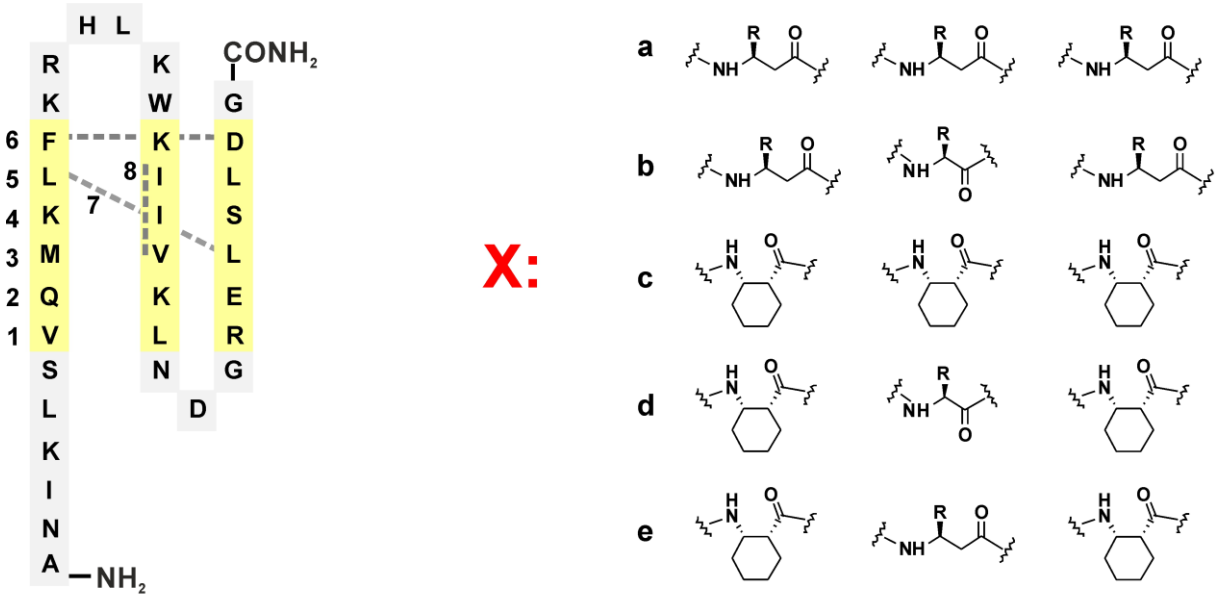

anginex-Gly	ANIKLSVQMKLFKRHLKWKIIVKLNDGRELSLDG-NH_2
1a-e	ANIKLS**X**QMKLFKRHLKWKIIVK**X**NDG**X**ELSLDG-NH_2
2a	ANIKLSV**X**MKLFKRHLKWKIIV**X**LNDGR**X**LSLDG-NH_2
3a-e	ANIKLSVQ**X**KLFKRHLKWKII**X**KLNDGRE**X**SLDG-NH_2
4a	ANIKLSVQM**X**LFKRHLKWKI**X**VKLNDGREL**X**LDG-NH_2
5a-e	ANIKLSVQMK**X**FKRHLKWK**X**IVKLNDGRELS**X**DG-NH_2
6a	ANIKLSVQMKL**X**KRHLKW**X**IIVKLNDGRELSL**X**-NH_2
7a	ANIKLSVQMK**X**FKRHLKWKI**X**VKLNDGRE**X**SLDG-NH_2
8a	ANIKLSVQMKLFKRHLKWK**XXX**KLNDGRELSLDG-NH_2

Figure 6. The designed anginex analogs. Substitution position is indicated by arabic numbers, starting with the first triplet (Val[7]-Leu[24]-Arg[28]) from the N terminal. Substitution pattern is indicated with dashed lines: **1**-**6** in registry substitutions, **7** – diagonal, **8** – sequential. The amino acids patterns in these positions (X, Y and Z) are indicated by letters: pattern **a** corresponds to β^3-homo-amino acid substitutions in all positions. Patterns **b**-**e** corresponds to β^3 and 1*R*,2*S*-ACHC substitutions only in the hydrophobic face of the peptide (positions 1, 3 and 5). Compound numbering is generated by the number of the substitution position with the letter of the substitution pattern.

In pattern **a**, open-chain β^3-amino acids were utilized, which allowed the retaining of the side-chain functionality and the pharmacophore points. Bioactivity variations could therefore be examined as a function of the structural changes. The tightly packed hydrophobic core may be disturbed by the extension of the backbone by one carbon atom at matching substitutions,

therefore in pattern **b**, only two residues were changed to β^3-amino acids in the peripheral strands of the hydrophobic positions (**1b**, **3b** and **5b**).

It has been shown that β^3-amino acids can adopt both *anti* and *gauche* torsion angles about the C^{α}-C^{β} bond in short turns, and the intramolecular H-bond pattern was found to be conformation dependent.[144] To achieve proper peptide bond orientation that fits the natural hydrogen-bonding pattern, *gauche* conformation is required. Molecular modeling suggested that in this case the side-chain overlap might be disturbed by the additional methylene group (Figure 7b). The desired gauche conformation can be fixed by using constrained amino acids, in pattern **c**-**e** therefore a conformationally constrained β-amino acid was tested in different arrangements. 1*R*,2*S*-*cis*-aminocyclohexanecarboxylic acid (1*R*,2*S*-ACHC) was chosen for substitution on the basis of stereochemical considerations: i) C^{β} configuration should match that of the natural amino acids and ii) six-membered saturated cyclic amino acid with *cis*-relative configuration in a β-sandwich structure gives a higher β-sheet content compared to other cyclic amino acid types.[87] This cyclic amino acid type also gave us the opportunity to investigate the contribution of the cyclic ring to the hydrophobic interactions, which might provide better overlap than that of the open-chain β^3-amino acids (Figure 7c). Pattern **c** contained three matching substitutions of the cyclic amino acid, and in pattern **d** the residues in the second strand remained unchanged. An additional mixed pattern was designed to test the compatibility of the open-chain β^3- and cyclic amino acids in the hydrophobic region of the peptide (**1e, 3e** and **5e**).

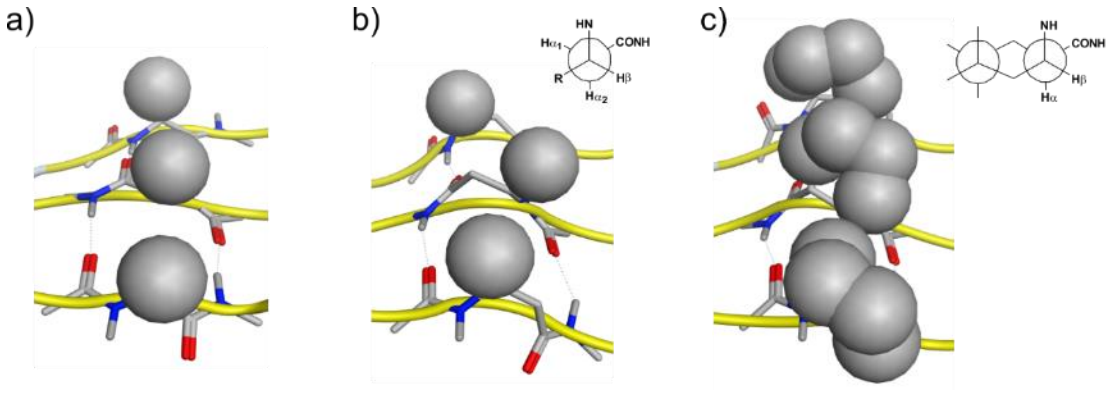

Figure 7. Comparison of the expected side-chain overlap of the **a)** original α-peptide sequence **b)** with matching β^3-amino acid substitutions in *gauche* conformation or **c)** matching 1*R*,2*S*-ACHC substitutions with fixed conformation.

With these 20 anginex analogs, the β-amino acid substitution effect on the local conformation, the overall β-sheet folding propensity along with hydrophobic interactions and

inducible folding could be investigated. The six-residue length of the β-sheet region of anginex enabled us to analyze the substitution effects vs. the distance from the turns and the effects on turn initiation. The core region contained various amino acids regarding hydrophobicity and side-chain branching, which allowed testing the tolerance of the different types of amino acids to substitution.

4.1.2. Optimization of peptide synthesis

Literature synthesis of anginex generally relies on standard solid phase peptide synthesis methods using Fmoc chemistry and automated peptide synthesizer without the utilization of special amino acids or coupling conditions.[117, 143] In our approach, in order to enhance the synthetic process and the coupling of the non-natural amino acid residues, microwave irradiation was utilized, which is known to accelerate the coupling and deprotection reactions.[145] Special conditions were applied to amino acids prone to racemization or byproduct formation.[146] Investigation of the sequence revealed a possible difficulty: the coupling of Asp^{26} to Gly^{27} might be particularly sensitive to byproduct formation under microwave irradiation due to its high propensity to form aspartimide, which is the result of a ring-closure between the β-carboxy side-chain of aspartic acid and the nitrogen of the previously coupled amino acid (Figure 8a).[147] This sequence-dependent side-reaction is catalyzed either by acids or bases and the branched side-chain protection groups (e.g. OtBu on aspartic acid) cannot prevent this. Furthermore, the repetitive base treatment required for deprotection steps during the synthesis increases the chance of this side-reaction.

Our initial approach utilizing factory settings and standard coupling reagents did not yield the required peptide; a shorter peptide fragment was identified via HPLC-MS/MS, which contained the anginex(25-33) sequence with a water loss. The termination of the synthesis at Asn25 was surprising, and the water loss suggested a ring-closed byproduct formation without a free N-terminal amine. Our hypothesis was that aspartimide formation between Asp^{26}-Gly^{27} might take part in the formation of this byproduct and the termination of the synthesis. In order to test this hypothesis, 0.1 M hydroxybenzotriazole (HOBt) was utilized in the deprotection solution, which had been shown to reduce aspartimide formation during microwave enhanced synthesis.[146] Under these conditions two additional products were detected: one with 18 Da less than the desired peptide, which indicated water loss caused by aspartimide ring formation, and the other with +67 Da, which corresponded to piperidide formation, which are well known modifications for aspartimide forming sequences (Figure 8a).[147] The reduced amount of the

terminated sequence pointed out that the preformed aspartimide ring was responsible for the termination of the synthesis.

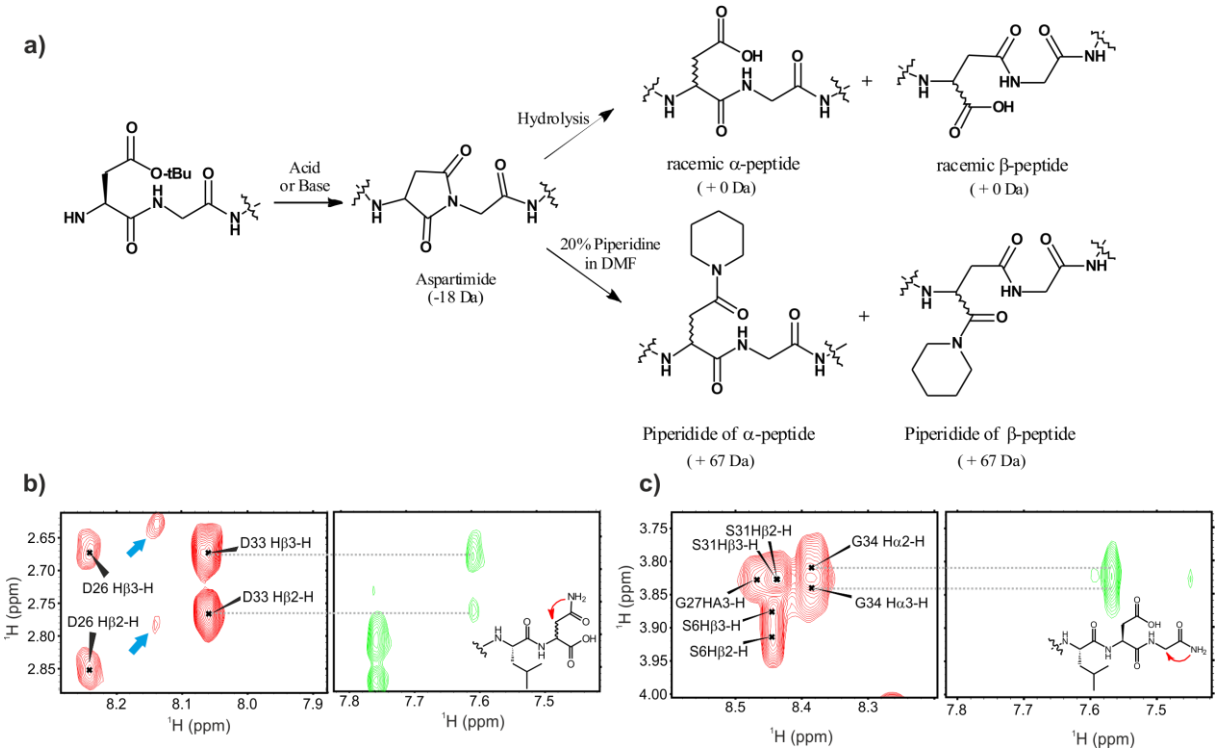

Figure 8. a) Mechanism of aspartimide formation between aspartic acid and glycine residues and the detected possible byproducts during the optimization of the microwave enhanced synthesis. Mass difference compared to the expected product is shown in brackets. **b)** NMR spectra of the product mixture after the first optimization. TOCSY (red) showing duplicated peaks for side-chain protons of the 33rd residue indicated by blue arrows and corresponding NOESY (green) spectra are showing the detected strong NOE interaction between H^{β} and side-chain amide with the hypothesized structure. **c)** TOCSY (red) and NOESY (green) NMR spectra of the product after the second optimization, having an extra glycine residue in the C-terminus (anginex-Gly). The detected NOE corresponds to the C-terminal amide Gly^{34} H^{α} interactions.

The most efficient synthetic approach to avoid aspartimide-related byproducts is the coupling of backbone amide protected glycine residue,[147] therefore in our next attempt the Fmoc-Asp(tBu)-(Dmb)Gly-OH dipeptide was used for coupling in the Asp^{26}-Gly^{27} position. MS measurements revealed the desired m/z value, analytical RP-HPLC however revealed one main product and three other byproducts with the same molecular weight, which suggested epimerization or β-amino acid formation after the hydrolysis of aspartimide ring both leaving the molecular weight intact (Figure 8a). NMR measurements of this mixture revealed a number of duplicated signals, with intensity proportional to the composition of the mixture. The most conspicuous signal split was found for Asp^{33}, which indicated a synthetic modification of this amino acid, and the commonly detected NOE between the C-terminal amide and H^{α} of the last residue was missing. Investigation of NOE interactions revealed strong NOEs between the H^{β}

protons of the 33rd residue and an unassigned amide proton (Figure 8b). The hypothesized mechanism for this is also based on an aspartimide formation during the synthesis between the side-chain of Asp[33] and the amide on the Rink Amide linker of the resin. The proximity of amide protons to the H^{β} of the 33rd residue and the missing NOE interaction pointed out that the ring opening occurred to form a β-peptide, which in this particular case could be also considered as an Asp to Asn and amide to free carboxyl group mutation in the C-terminus.

Our attempts to avoid this side-reaction could be resolved only with the coupling of the protected dipeptide in the last position of anginex, which resulted in a glycine extension on the C terminus of the peptide (anginex-Gly). In this case, the RP-HPLC revealed only one product and the NMR spectrum did not contain any duplicated signals. The common strong NOE interaction between the C-terminal amide proton and Gly[34] H^{α} protons was found in this case (Figure 8c), which suggested the formation of the expected product. All analogs were synthesized successfully under these optimized conditions and contained Gly[34] modification in the C-terminus except for **6a**, where Asp[33] was substituted with β^3-hAsp, which also eliminated this side-reaction.

4.1.3. Conformation at the residue level by NMR

Optimization of measurement conditions

In order to gain insight into the local conformational preferences of the replaced amino acids, structural analysis was carried out by NMR. The β-sheet folding of anginex and related peptides are highly sensitive to measurement conditions, NMR measurement of these peptides may suffer from poor quality spectra due to aggregation or interchange between different conformations,[18] the measurement conditions had to be therefore optimized to obtain high quality data.

β-Sheet folding can be tuned by a number of different conditions such as pH, temperature and other additives. Generally, pH closer to neutral with elevated temperature enhances hydrophobic forces and the β-sheet fold can be observed. This can be followed by downfield shifted H^{α} and NH protons in the ^1H spectrum.[148] High resolution structure of anginex was determined at 1 mM peptide concentration in a H_2O:DMSO 1:1 mixture, pH 5.5 and 40˚C after addition of 50 mM DPC.[110] In our hand, these conditions did not result in reasonable spectra.

At pH 5.6 and 500 μM peptide concentration at 37 °C, the ^1H spectrum of anginex-Gly showed sharp peaks and narrow chemical shift distribution, which indicated mainly random coil conformation (Figure 9a). Increasing the pH to 7.4 or after addition of DPC caused

downfield shift of NH and H^{α} resonances, which were observed at around 8.5 - 9.5 and 5 - 6 ppm indicating well folded β-sheet regions (Figure 9 b,c). Signal assignment was prevented by resonance broadening under these conditions, which might arise from the slow chemical exchange between the folded and unfolded populations.[18] For chemical shift assignment, spectra were therefore recorded at pH 5.6, 37 °C in the absence of DPC, which yielded high quality spectra but high resolution structure could not be determined due to the large part of unfolded population.

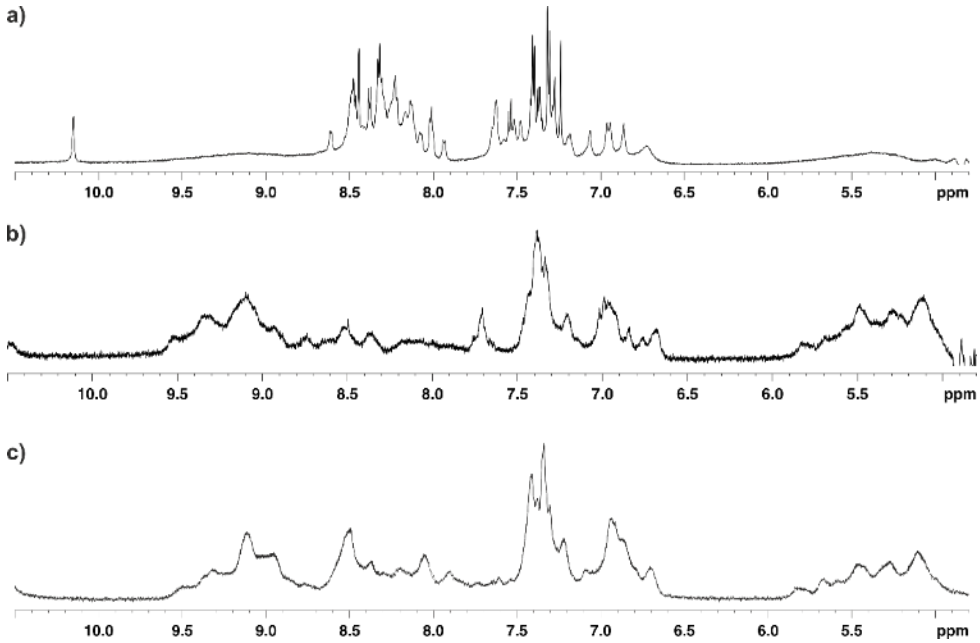

Figure 9. ^{1}H-NMR spectra of anginex-Gly under different measurement conditions using 500 μM peptide concentration. **a)** pH 5.6 at 37 °C showing mainly random coil conformation**, b)** pH 7.4 at 37 °C and **c)** pH 5.6 + 12.5 mM DPC. The downfield shifted H^{α} and NH protons indicate well-formed β-sheet parts.

Homonuclear TOCSY and NOESY spectra were used to assign NH and H^{α} chemical shifts and heteronuclear ^{13}C-HSQC to assign C^{α} and C^{β} chemical shifts (Figure 10). ^{13}C-HSQC was measured in pure D_2O with the same buffer in order to eliminate water signal. In this way the majority of the chemical shifts were assigned except for NH chemical shifts for Ala^{1} and His^{15} in some cases. The assignments were suitable for the investigation of local conformational preferences of the amino acids, which gave us insights to turn stability and the conformation of β-amino acids. Chemical shift analysis resulted in information about the secondary structure forming propensity.

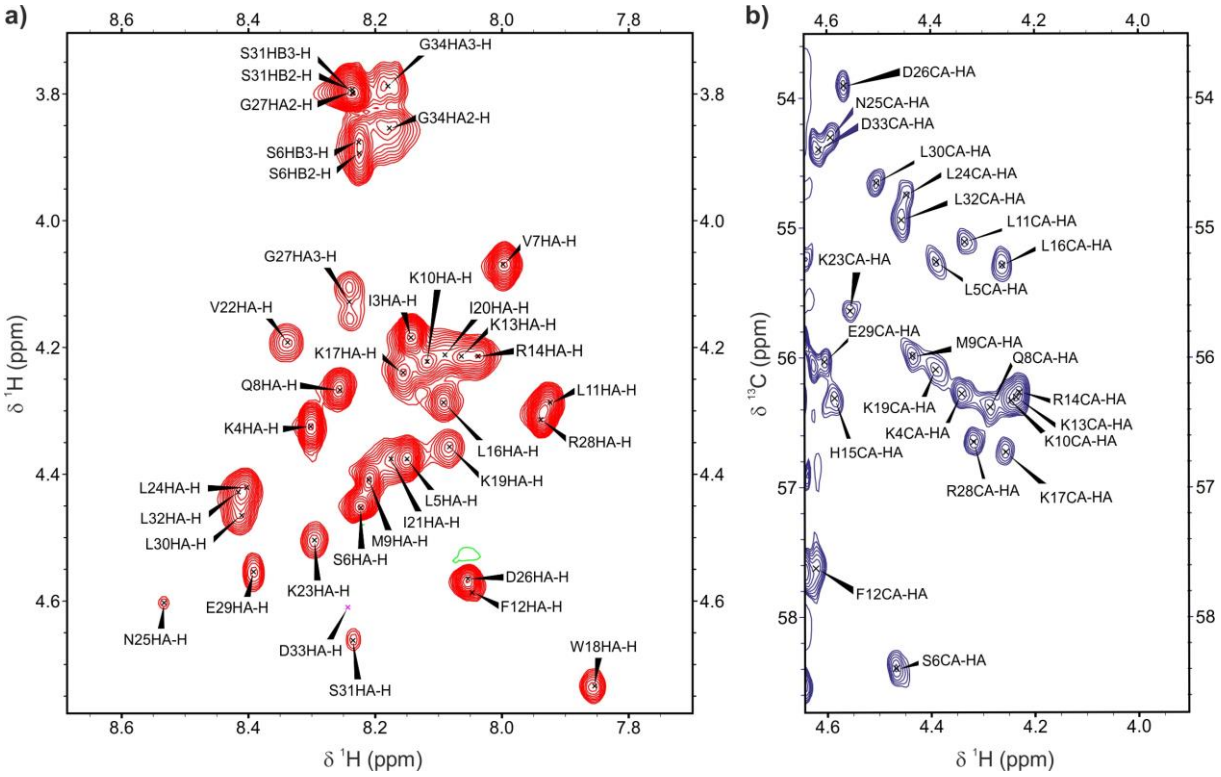

Figure 10. **a)** H^{α}-NH region of TOCSY spectrum of anginex-Gly **b)** ^{13}C-HSQC spectrum part showing assigned C^{α} chemical shifts.

Turn initiation

Turn initiation plays an important role in early folding as it is responsible for the preorganization of the proper side-chain alignment along the strand, improper turn initiation may lead to misfolded or unfolded structure. Turn residues were not substituted, but the effect of close substitutions on turn stability might provide useful information on the role of the rigidity of the loops. Turn rigidity can be indicated by the chemical shift difference ($\Delta\delta$) of the diastereotopic protons of a glycine residue, and in the case of anginex-Gly, the second, tighter turn contains a glycine residue (Gly^{27}, Figure 11a). Generally, substitutions closer to this turn segment resulted in decreased $\Delta\delta$ values (Figure 11b), which indicated higher flexibility. The effects of different amino acid types on the turn stability were not apparent except for analogs **1c-e**, which suggested that the loss of side-chain functionality, especially Arg^{28}, resulted in highly destabilized turn segment. The reason for the structural instability upon substitution of Arg^{28} may be the loss of a potential turn stabilizing salt bridge.

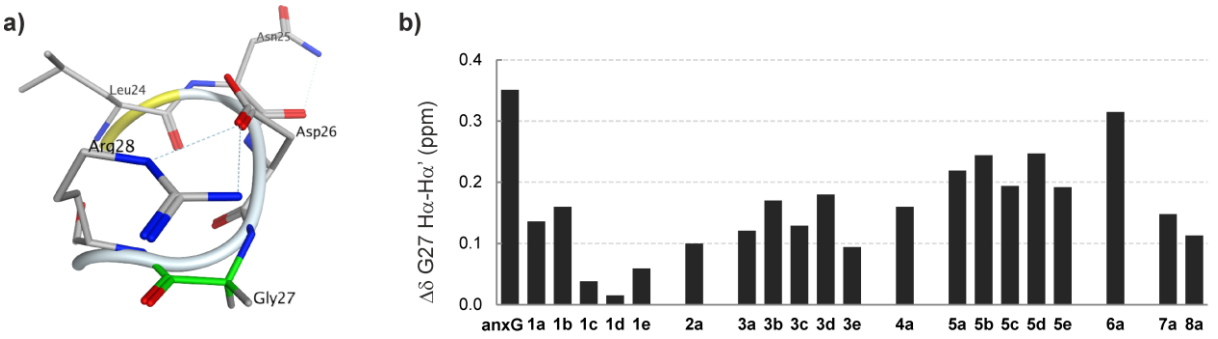

Figure 11. **a)** Model of the second turn Gly[27] residue is highlighted by green color. **b)** Diastereotopic proton chemical shift difference of Gly[27] in all analogs, indicating the rigidity of the second turn anginex[25-27] of anginex analogs.

None of the analogs reached the Δδ value of anginex-Gly, which indicated higher structural flexibility. The substitution-position dependence of the turn rigidity suggested that core substitutions had the lowest effect on turn initiation.

Hydrogen bond pattern – local conformation of β[3]-amino acids

Proper orientation of amide bonds plays a key role in the formation of the complementary hydrogen-bond pattern between the strands. The extra carbon atom in the β[3]-amino acids may increase the flexibility of the corresponding residue, and results in a non-matching conformation to the hydrogen-bond pattern. To test the rigidity of β[3] residues in the sequence, the chemical shift difference of the diastereotopic H[α] protons of the β[3]-amino acids were investigated. The Δδ values were dependent primarily on the substituted amino acid type regardless of the substitution position and the pattern used. Generally, the Δδ values for β[3]-amino acids, which contained side-chain branching (β[3]hVal- and β[3]hIle-residues) were in the range 0.14–0.24 ppm, *i.e.* systematically higher than the average Δδ (0.10 ppm), indicating increased local rigidity (Figure 12).

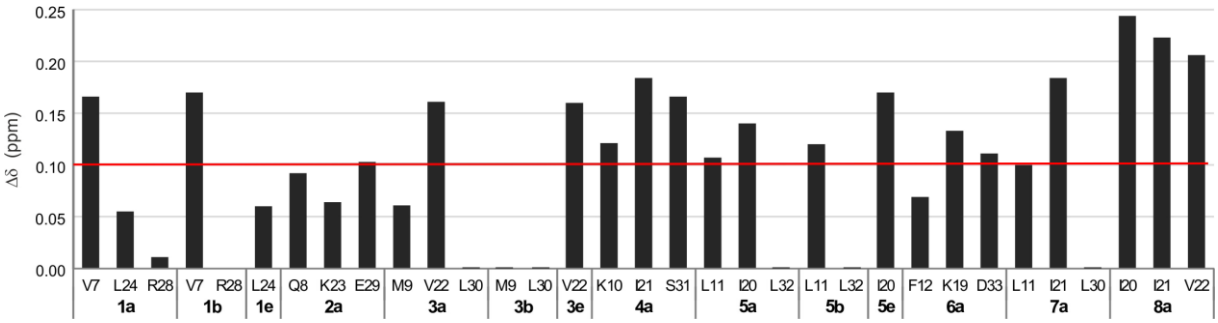

Figure 12. Δδ values of diastereotopic H[α] protons of the β[3]-amino acids. The red line indicates the average Δδ value. Single letter amino acid codes indicate the substitution position in the corresponding peptide.

Residues that displayed increased local rigidity was subjected to further conformational analysis by investigating the $^3J(H^{\alpha}\text{-}H^{\beta})$ couplings and the Hα-NH NOE intensity patterns around these residues. β[3]-Amino acids can attain three possible conformations*: gauche -*, *anti* and *gauche +* (conformations *g-*, *anti* and *g+* in Table 2). *Gauche +* conformation is compatible with the hydrogen bonding pattern of the β-sheet.

Large $^3J(H^{\alpha 1}\text{-}H^{\beta})$ (>10 Hz) values were uniformly accompanied by elevated $I_{NOE}(H^{\alpha 1}\text{-NH})/I_{NOE}(H^{\alpha 2}\text{-NH})$ ratios in most of the residues, indicating a conformational bias toward the local conformation C. On the other hand, the backbone curvature caused by this conformation suggested that these homo-amino acids did not fit properly into the tightly packed core of anginex.

Table 2. Local conformational analysis of residues with increased rigidity; the three possible conformations are indicated with *g-*, *anti* and *g+*.

Comp-ound	Substiuted residue	$J^3_{H^{\beta}\text{-}H^{\alpha 1}}$ (Hz)	$J^3_{H^{\beta}\text{-}H^{\alpha 2}}$ (Hz)	NOE integral ratio $I(H^{\alpha 1}\text{-NH})/I(H^{\alpha 2}\text{-NH})$	Confor-mation
1a	V7	10	5	2.9	*g+*
1b	V7	10[b]	6[b]	9.4	*g+*
3a	V22	12	4	4.5	*g+*
3b	V22	12	4	2.3	*g+*
4a	I21	11	5	2.4	*g+*
	S31	9	5	3.0	*anti / g+*
5a	I20	10	6	1.7	*anti / g+*
5b	L11	9	7	1.0	*anti*
5e	I20	11	7	2.4	*g+*
6a	K19	7.5	7	1.4	*anti*
7a	I21	11[b]	4	2.5	*g+*
8a	I20	10	6.5[b]	1.9	*g+*
	I21	9	7[b]	1.1	*anti*
	V22	11.5	5.5[b]	2.6	*g+*

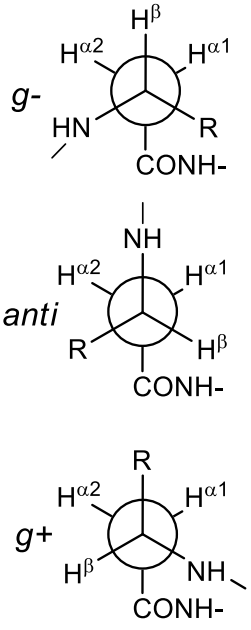

This observation was in line with the literature results which showed that side-chain branching adjacent to the β-carbon atom stabilized the 14-helix,[149] which is possible only if there is a propensity to attain a *gauche* θ torsion suggesting the use of constrained amino acids. Fixing the desired conformation could be advantageous for the proper amide bond and side-chain orientation.

Secondary structure propensity

In order to gain deeper insight into the β-sheet forming propensity at the amino acid level, and to examine the effects of the flexible and the constrained residues, chemical shift analysis[150-151] was utilized. The chemical shifts of the backbone nuclei depend on the dihedral

angles ψ and φ of the residue, thus they are affected by the secondary structure.[152] NH, H^{α}, and C^{β} chemical shifts exhibit a downfield shift, whereas C^{α} chemical shifts display an upfield shift upon β-sheet formation, and the opposite change is observed for helices.[153]

First, a qualitative investigation of the chemical shifts of the core amino acids was carried out. The β-sheet core of anginex contains hydrophobic Ile and Val residues in the second strand, which may be particularly indicative of β-sheet folding, also the C^{α} chemical shift of these residues are usually not in overlap with other types of amino acids, making the analysis easier. Comparison of the C^{α} and H^{α} chemical shifts of Ile and Val residues in anginex-Gly and its analogs revealed primarily substitution position-dependent changes. The chemical shift of Ile^{21} was highly affected by the substitutions and exhibited downfield shifted C^{α} by 0.4-0.7 ppm and upfield shifted H^{α} resonances by 0.2-0.4 ppm compared to those of the parent peptide (Figure 13). This pointed to the loss of β-sheet structure and to the importance of this residue to stabilize the hydrophobic core region. Both Ile^{20} and Val^{22} showed similar behavior upon substitutions, but to smaller extent. Amino acids far from the β-sheet core (Ile^{3}) exhibited only minor changes. The chemical shift change of Val^{7}, which is part of the first, most flexible region of anginex exhibited substitution type dependence. β^3-Amino acid substitutions resulted in downfield shifted C^{α} and upfield shifted H^{α} resonances indicating the loss of β-sheet structure. Contrary to this, 1*R*,2*S*-ACHC substitutions led to an opposite change indicating higher propensity to form β-sheet strand. This may be explained by the conformational preferences of the different types of amino acids and by the preorganized conformation of the constrained amino acid.

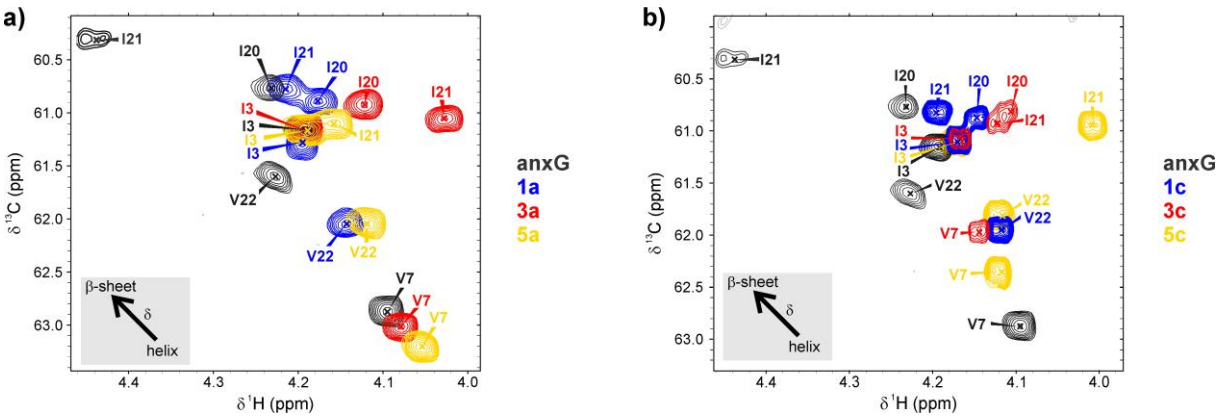

Figure 13. Representative part of the ^{13}C-HSQC of Val and Ile C^{α}-H^{α} region for analogs with **a)** β^3-amino acid substitutions in the hydrophobic face and **b)** 1*R*,2*S*-ACHC substitutions. Arrows in the lower-left corner indicate the expected secondary structure-dependent chemical shift change.

To gain information on all amino acids, secondary chemical shift analysis was carried out, which could be used to detect transiently formed secondary structures. This was shown to be a

general approach for intrinsically disordered proteins.[153-154] Secondary chemical shift analysis is based on the difference between the experimentally determined and a set of random coil chemical shifts ($\delta - \delta^{rc}$) indicating positive or negative deviations from a reference random coil value, respectively.[155] The accuracy of the analysis depends on the selected reference random coil chemical shift set. In our case, the reference random coil chemical shift set was based on values obtained for small peptides corrected for the pH, temperature and the effects of the neighboring residues.[154, 156] The chemical shift differences were calculated for H^{α}, NH, C^{α}, and C^{β} chemical shifts (Figure 14).

Among all investigated nuclei, the secondary chemical shift of H^{α} resonances of anginex-Gly exhibited the highest correlation with the literature structure. Positive values were calculated for residues 17-25 and 29-32 that are part of the second and third strand respectively, which pointed to a transiently formed β-sheet structure. Secondary chemical shifts of C^{β} and C^{α} showed similar tendencies, whereas NH resonances revealed high variability, suggesting that the latter one was a poor predictor of secondary structure formation. The complexity of this data enabled us to observe only general effects of the different substitutions. The calculated secondary chemical shifts of the analogs revealed a strong substitution position-dependence on β-sheet forming propensity and the effect of the substituted amino acid type seemed to be of secondary importance (Figure 14).

Generally, the NH chemical shifts were the least affected by the substitutions in all cases. Systematic decrease in secondary chemical shifts were observed for all nuclei near β-amino acid substitutions, which indicated the loss of β-sheet propensity compared to that of the parent peptide, although the structure-independent neighborhood effect of the β-residues on the magnetic environment of the adjacent α-residues could not be ruled out either. β^3-substitutions increased the helix forming propensity of the first strand, which was more prominent on the H^{α} and C^{α} chemical shifts of analogs with substitutions on the hydrophobic face (**1a, 3a, 5a,** Figure 14a). The highest β-sheet forming propensity was measured for **6a** (Figure 14b) and Hα and C^{α} chemical shifts of non-matching substitutions exhibited a high β-sheet loss (Figure 14c).

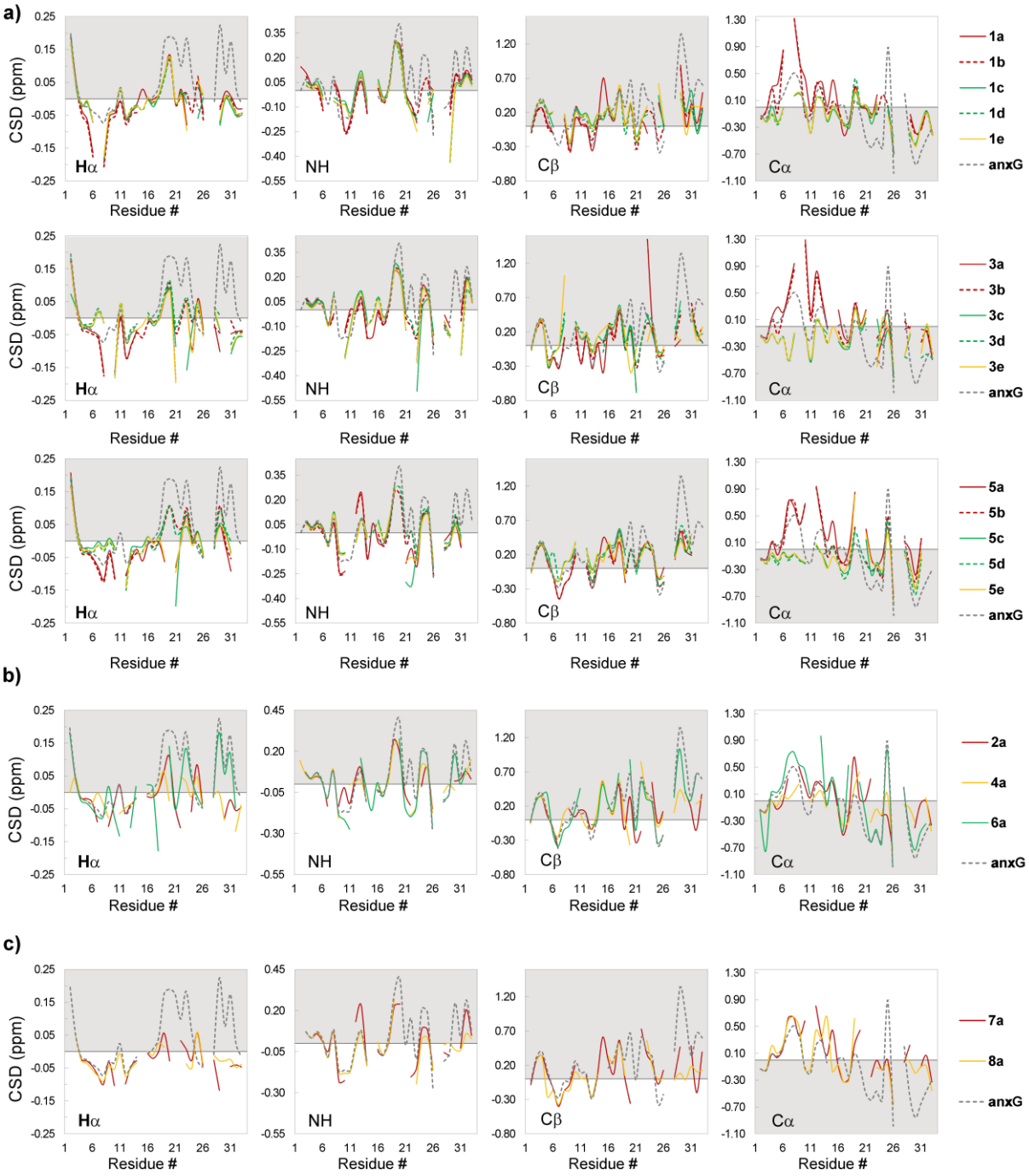

Figure 14. Envelopes of chemical shift difference for H^{α}, NH, C^{β}, C^{α} of the analogs with substitutions on the **a**) hydrophobic face of the peptide, **b**) on the hydrophilic face and **c**) non-matching substitutions. Values in grey shading (positive values for H^{α}, NH, C^{β}, and negative values for C^{α}) indicate β-sheet formation. Chemical shift difference was calculated by subtraction of a predicted reference random coil chemical shift from the measured data.

In order to facilitate the comparison of the secondary structure propensities, all chemical shifts were combined into the secondary structure propensity (SSP) scores, which were calculated by using the SSP program.[157] The resonances of β-amino acids and glycines were excluded because of the lack of reference values and C^{β} chemical shifts, respectively. For this

calculation, a different random coil chemical shift reference set, based on protein assignments (refDB) was used that was included in the software without correction to pH or temperature.[158] Nevertheless, the results correlated well with the secondary chemical shift values observed for the individual nuclei. SSP score values vary between 1 and -1 showing helix or β-sheet forming propensity respectively (Figure 15).

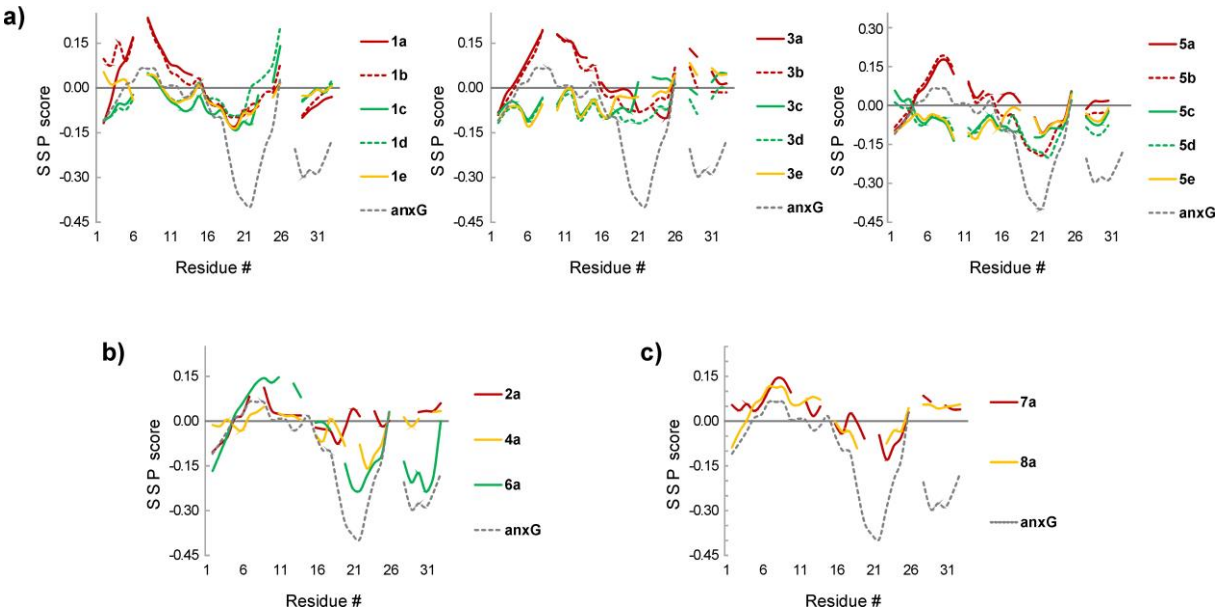

Figure 15. Envelopes of SSP scores indicating folding propensities for substitutions in **a)** the hydrophobic face, **b)** the hydrophilic face and **c)** non-matching positions. Positive and negative values correspond to helix and a β-sheet propensity, respectively.

Without induction, anginex-Gly showed moderate β-sheet propensity with calculated SSP scores of -0.2 to -0.4 for the second and third strands. We found values around zero for the first strand indicating random conformation in line with the earlier observation that the first strand of the β-sheet was more flexible than the other two.[110] Generally, SSP values were lower than that of the parent peptide, all β^3 substitutions resulted in induced helical propensity in the first strand, which could be explained by the helix promoting tendencies of these building blocks and the flexibility of this segment. These suggested that the amino acid replacements had a strong effect on the secondary structure propensity of an entire chain segment. 1*R*,2*S*-ACHC substitutions diminished this tendency and turned it into a β-sheet forming propensity, which suggested that the preorganized conformation of the cyclic amino acid residue promoted an extended chain conformation that could be advantageous for strand formation.

In the hydrophobic face, different substitution pattern preference was found depending on the substitution position (Figure 15a). In position 1, matching 1*R*,2*S*-ACHC substitutions were most tolerated (**1c**), whereas in the third strand, analogs with maintained side-chain chemistry

exhibited the highest β-sheet propensity (**1a** and **1b**). In position 3 only the peripheral cyclic amino acid substitutions were tolerated (**3d**), which indicated that the β-sheet core was highly sensitive to modifications. In position 5, both the peripheral β^3 and cyclic replacements exhibited β-sheet forming propensity (**5b** and **5d**), which indicated a better fit of the side-chains to the hydrophobic core in this position.

On the hydrophilic face, β^3 substitutions are tolerated well in the peripheral regions of anginex-Gly (Figure 15b); **6a** exhibited the highest β-sheet content. The β-sheet folding tendency of non-matching substitutions were similar to hydrophobic core substitutions (Figure 15c), which might arise from impairment of hydrophobic side-chain orientations rather than from the demolished hydrogen-bond interactions.

^{1}H-NMR spectra exhibited similar resonance broadening that was observed for anginex after provision of the structure-inducing DPC. This prevented signal assignment and high resolution structure analysis. Several analogues showed downfield shifted H^α, and NH resonances, which indicated β-sheet formation; the most pronounced change was observed for **1d** (Figure 16a,b). Moreover H^α-H^α NOEs, representative for β-sheet hydrogen-bond pattern were observed also for **1d** (Figure 16c).

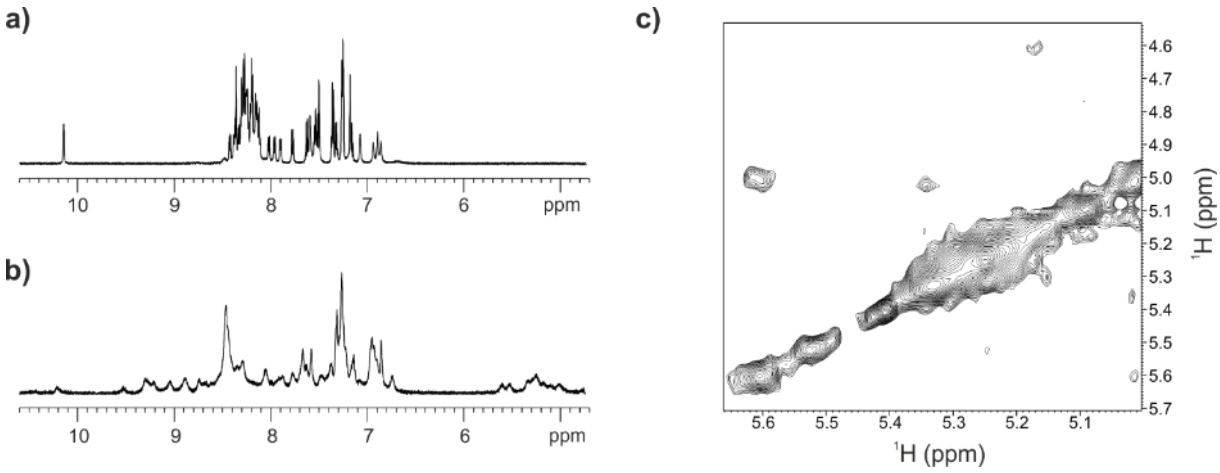

Figure 16. a) ^{1}H NMR spectrum of **1d** in 500 μM peptide concentration pH 5.6 HEPES, 37°C and **b)** after addition of 12.5 mM DPC, which caused downfield shifted NH and H^α resonances, indicating well-formed β-sheet parts. **c)** 2D-NOESY spectrum of **1d** indicating H^α-H^α NOEs of β-sheet origin.

4.1.4. Overall folding

Overall folding tendencies of the analogs were investigated via CD spectroscopy with and without the membrane mimicking DPC. The effects of β-amino acid substitutions on CD signals are not exactly known; however only 5-9 % of non-natural residue content is present in the analogs, therefore the CD curves are expected to resemble those of the natural peptide

sequences. The experimental conditions were chosen to maintain the solubility of the peptides and keep the background absorbance low, therefore experiments were carried out in K-phosphate buffer at pH 5.6 using 100 μM peptide concentrations. For the investigation of the induced folding, membrane mimicking environment was provided by using DPC at 2.5 mM concentration, which is 25-fold excess to the peptide concentration and above its critical micelle concentration,[159-161] to ensure micelle formation.

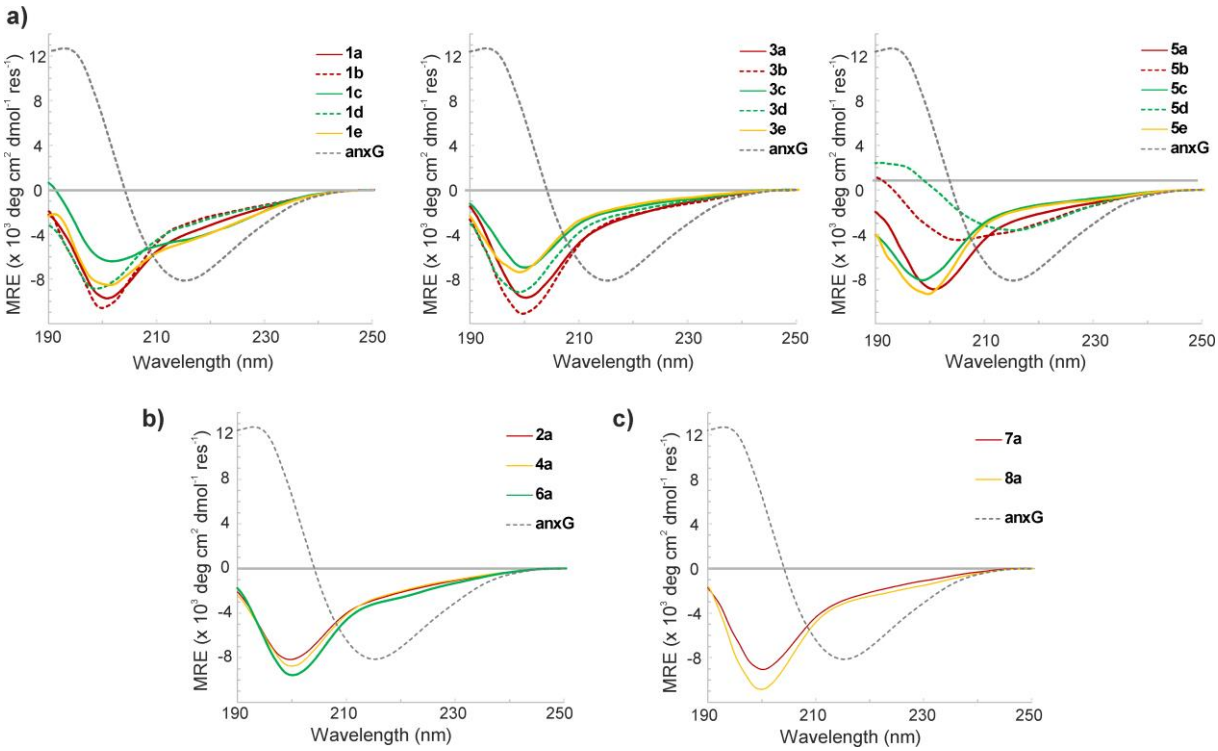

Figure 17. CD curves of anginex-Gly (anxG) and analogs at 100 μM peptide concentration in pH 5.6 K-phosphate buffer, 37 °C **a)** analogs with substitution in the hydrophobic **b)** in the hydrophilic face and **c)** non-matching substitutions.

In buffer only, the CD curve of anginex-Gly at 100 μM concentration showed a Cotton effect at 215 nm, which was consistent with β-sheet folding (Figure 17). The CD traces of most of the analogs without induction shared a common minimum at around 200 nm and had a shoulder at 217 nm with variable intensity, which suggested partial folding. The slight differences of the CD curves of analogs with substitutions in the hydrophobic face suggested that the substitution pattern might have a substantial effect to the overall folding. The CD curve of **5b** and **5d** displayed significant β-sheet fold, and exhibited minima at 210 and 217 nm respectively (Figure 17a). Substitutions in the hydrophilic face (**2a, 4a, 6a**) and the off-registry patterns (**7a, 8a**) resulted in highly similar CD curves, which suggested that substitutions in these positions had a similar effect on the secondary structure (Figure 17b,c).

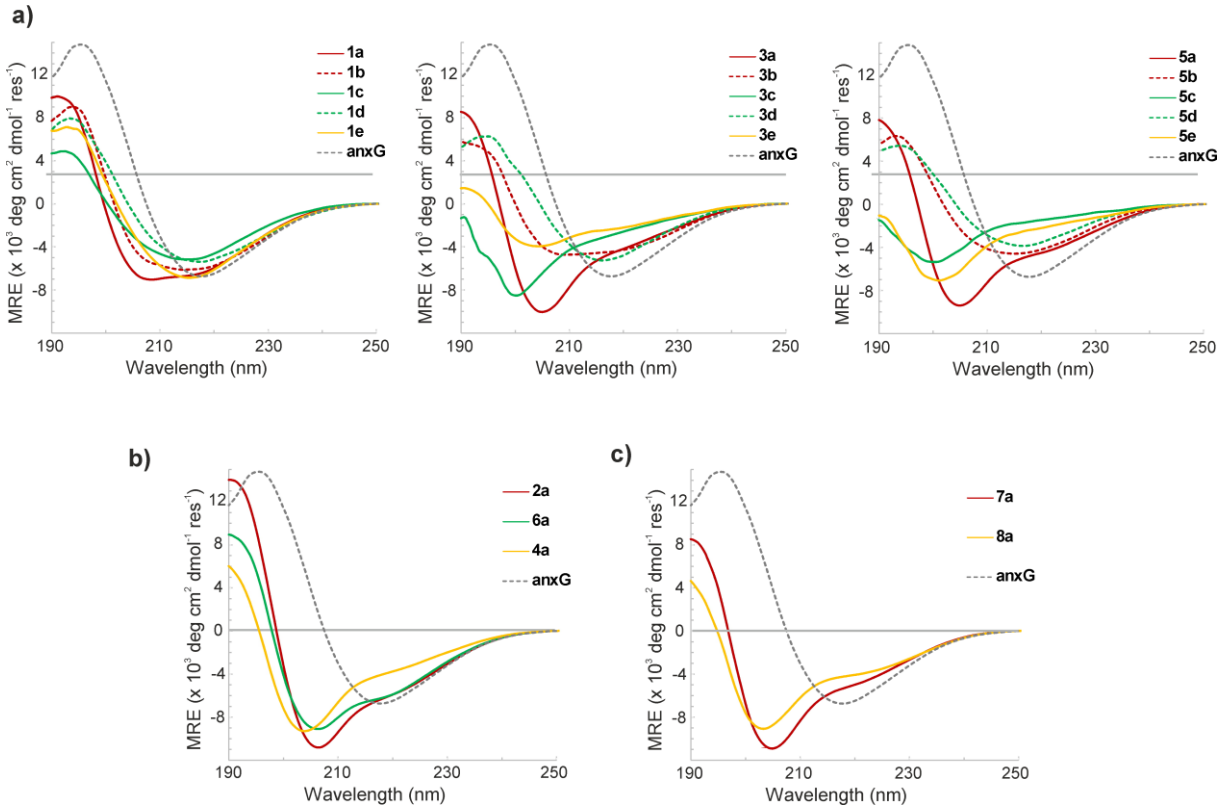

Figure 18. CD curves of anginex-Gly (anxG) and analogs at 100 μM peptide concentration in pH 5.6 K-phosphate buffer, 37 °C after the provision of the membrane mimicking DPC at 2.5 mM concentration. **a)** Analogs with substitution in the hydrophobic **b)** in the hydrophilic face and **c)** non-matching substitutions.

The shape of the CD curve of anginex-Gly did not change significantly after the provision of membrane mimicking environment by DPC. The minimum shifted toward 218 nm and the intensity slightly increased, which suggested β-sheet formation upon interaction with DPC. The structuring effect of DPC was clearly apparent in the CD curves of all analogs, which exhibited strong substitution position dependence. Substitution position close to the turn region of anginex (**1a-e**) exhibited the highest change upon induction and all substitution patterns resulted in increased β-sheet formation in a similar extent (Figure 18a). Closer to the β-sheet core in the hydrophobic face, patterns **b** and **d** were the most tolerated (**3b, 3d**, and **5b, 5d**). This may be explained by the maintained hydrophobic core in the middle strand. Matching β^3-amino acid substitutions in the hydrophilic face resulted in an increased shoulder at 217 nm and the minimum shifted toward 210 nm with a zero cross-point around 200 nm (Figure 18b), which indicated partial folding. Sequences **7a** and **8a** did not show a significant difference from the in-registry mutated analogs (Figure 18c), indicating that there was no extra sheet-breaking effect due to the non-matching local conformational behavior of the β- and the surrounding α-residues. These CD curves also showed similarities to helical conformation, but without the

characteristic intensities of the α-helix, which might be explained by the partial helix formation propensity of the N-terminus as revealed by NMR.

Quantitative estimation of secondary structure content

In order to estimate the secondary structure content quantitatively on the basis of the experimental CD curves, convex constraint algorithm (CCA+) analysis was carried out.[138-139] All CD data including the non-induced, the induced and temperature dependent measurements were included in the analysis and deconvoluted to three component curves. The components were assigned on the basis of similarity to reference CD curves of the pure peptide secondary structures[162] (Figure 19a). The first component had a minimum around 205 nm and resembled most the random coil structures. The second component exhibited a minimum around 217 nm, this was assigned to a folded β-sheet structure. The third component exhibited two minima at 205 and 220 nm, which did not show the characteristic intensities of a CD curve of an α-helix, but it could be assigned to short helical segments. This CD curve also showed close similarity to the traces of the DPC induced analogs that contained only β^3-amino acid replacements (**1a-8a**), which indicated that this third component originated from these analogs, and might be the effect of β^3-amino acid replacements on local conformation.

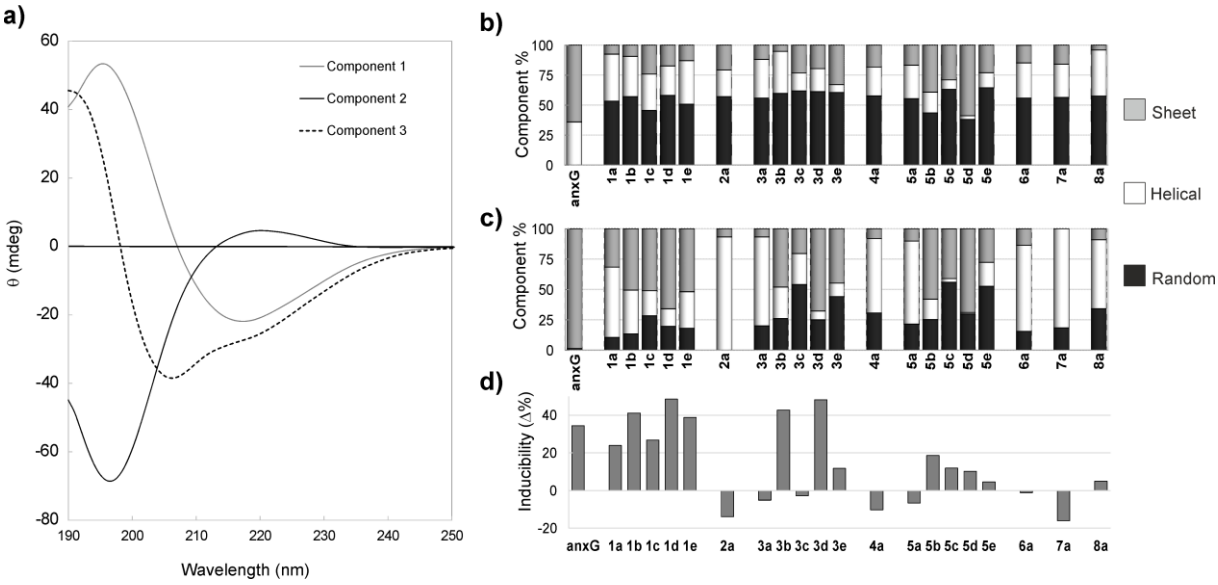

Figure 19. a) Results of the CCA+ deconvolution analysis yielding 3 pure component CD curves. The curves were assigned as follows: component 1: random coil, component 2: β-sheet, component 3: short helical segments. **b)** Secondary structure content in percentages of the analogs without induction and **c)** after induction with 2.5 mM DPC. Grey bars indicate β-sheet, white bars indicate helical and black bars corresponding to random coil secondary structure content. **d)** β-Sheet inducibility for all analogs that is calculated by the difference in initial and induced β-sheet content and expressed in Δ%.

The secondary structure contents were given as fractions of the 34-mer peptides; anginex-Gly showed ~64% β-sheet content, which increased to ~98% upon addition of DPC (Figure 19b,c). The calculated distributions of the secondary structure elements were in line with the observed CD curves. The population of the secondary structure elements was found to be dependent on the substitution position. Wide diversity was observed in β-sheet content for the analogs: 5-64% in solution and 20-98 % after addition of DPC. The extent of change in β-sheet content, regarded as inducibility, varied between -13 to +49 % (Figure 19d). Three different behaviors could be distinguished based on the initial β-sheet fold and inducibility: i) low initial β-sheet content accompanied by low inducibility; ii) low initial β-sheet but high inducibility and iii) high initial β-sheet without further inducibility.

In the first group, analogs exhibited initial β-sheet content below 25%, which could not be induced further by providing DPC. These were generally observed with triplet β^3-amino acid **(2-8a**) or triplet core 1*R*,2*S*-ACHC substitutions (**3c**, **3e, 5c** and **5e**), which suggested that these strategies are detrimental to the β-sheet fold. In the second group, analogs displayed low initial β-sheet content, but the membrane mimicking environment had high impact on folding and β-sheet content increased by more than 20 % upon induction. This was generally observed with substitutions near the second turn (**1a-e**) or in the peripheral regions (**3b**, **3d**), which suggested that the β-sheet stabilizing forces were missing without induction. This may arise from the turn instability or improper initial side-chain orientation, but after induction they may fit to the hydrogen-bond pattern and hydrophobic core. The third group exhibited an initial β-sheet content higher than 25 %, which could not be further increased by the membrane mimicking environment, this was observed in the case of **5b** and **5d** and suggested good initial fit to the hydrogen-bond pattern and side-chain packing.

These data revealed that the extent of β-sheet content depended on both the substitution position and the substituted amino acid type. Findings suggested that substitutions in the middle strand were not preferred, but tolerated in the peripheral region, which might be due to the inability of the β-amino acids to fit into the tightly packed hydrophobic core of the β-sheet. On the other hand, the creation of a hydrophobic cluster near the turn segment resulted in highly inducible structures.[87]

Hydrophobic interactions and self-association

Favorable side-chain pairings provide a hydrophobic core for the β-sheet, and the interactions between the laterally paired side-chains are a main driving force of folding. These hydrophobically driven interactions scale up with temperature,[163] which allows the evaluation of the presence of the solvophobic stabilizing forces using temperature dependent measurements. CD measurements carried out in range 5 – 75 °C in 5 °C steps without induction revealed a maximum intensity of the negative minimum at 217 nm for anginex-Gly at 60 °C, which pointed out that this was the optimum temperature for β-sheet folding (Figure 20a). Lower temperatures resulted in cold denaturation and a decrease in β-sheet content as observed for a number of anginex related peptides.[108] The decreased ellipticity and β-sheet fold at higher temperatures could be attributed to structural melt caused by thermal denaturation. Most of the analogs exhibited constant rising of the intensity at 217 nm without structural melting (Figure 20b). This may be explained by the presence of the hydrophobic interactions, however the lack of cooperative folding. Analogs that exhibited higher initial β-sheet folding (**5b** and **5d**) exhibited a similar biomimetic behavior as observed for the parent peptide (Figure 20c).

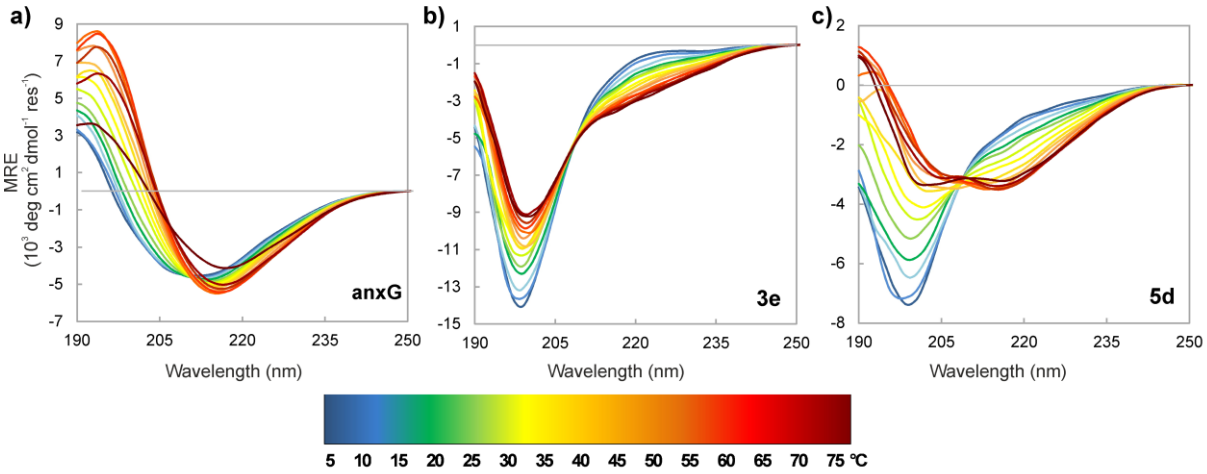

Figure 20. Representative examples of temperature dependent CD measurements. **a)** anginex-Gly **b) 3e** exhibiting constant rising in intensity at around 217 nm and **c) 5d** that exhibited similar biomimetic behavior as observed for the parent peptide.

This phenomenon could be followed on the deconvoluted CD spectra by comparing the relative β-sheet content changes (Figure 21). Temperature dependent CD curves were deconvoluted by the CCA+ software and the slopes of β-sheet content change relative to the starting temperature were analyzed with the assumption that higher slopes might be indicative of higher hydrophobic contribution to the folding. The β-sheet content of anginex-Gly increased by 27 % upon rising temperature, which was the highest of all peptides. Most of the analogs exhibited a monotonous enhancement in β-sheet content from 5 °C to 75 °C and exhibited

different slopes. The hydrophobic effects were generally scaled down in most of the analogs, which suggested that this phenomenon highly contributed to the structure breaking effect of β-amino acids.

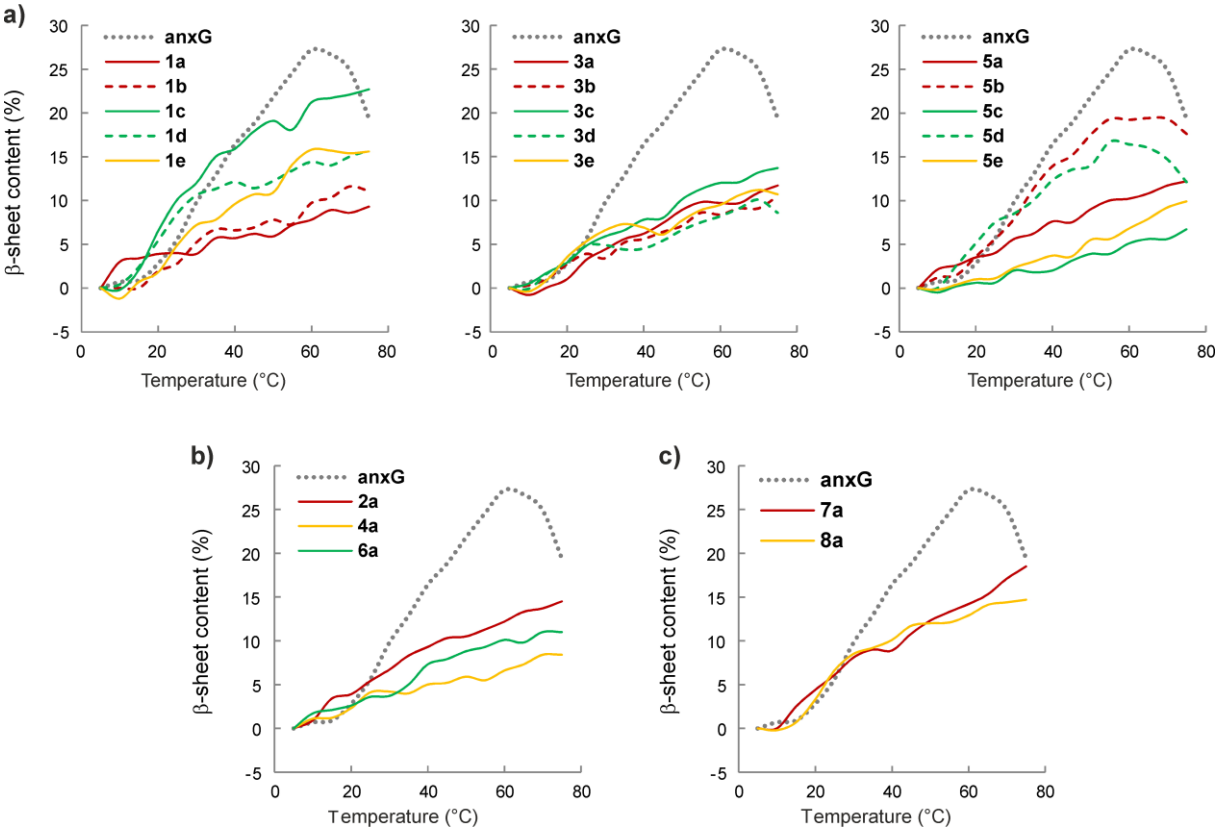

Figure 21. Change in β-sheet content of analogs with substitutions on the **a)** hydrophobic **b)** hydrophilic face and **c)** non-matching substitutions in response to increasing temperature. β-Sheet contents were determined by using CCA+ deconvolution. Displayed curves are normalized to the β-sheet content observed at the starting temperature (5°C) by subtraction.

In the hydrophobic substitution positions (Figure 21a) the increase in β-sheet content reached 15-22% of analogs with 1*R*,2*S*-ACHC substitutions near the turn segment (**1c, 1d** and **1e**), which pointed out that the hydrophobic cluster provided by the cyclic side-chains made a higher contribution to the stabilizing interactions near the turn segment. This was in line with the observation that hydrophobically driven stabilization was more pronounced in β-hairpins in which the hydrophobic cluster was close to the turn.[104] The hydrophobic cluster of the cyclic amino acids may provide a compensation for the substitution-induced turn destabilization as revealed by NMR. Substitutions in the core of the β-sheet (**3a-e**) resulted in highly decreased hydrophobic stabilization regardless of the amino acid type. This could be explained by the inability of the β-residues to fit into the tightly packed hydrophobic core. In the third hydrophobic position **5d** and **5e** showed signs of structural melt, which might arise from the

proper fit of the side-chains into the tightly packed core regions. The unique behavior of **5b** and **5d**, highlighted that β^3-homoleucine (β^3hLeu) or 1*R*,2*S*-ACHC substitutions in positions with similar solvent exposed surface compared to the original amino acid leucine resulted in high predominant β-sheet content and minor conformational change upon induction, which highlighted the importance of side-chain compatibility with the hydrophobic core.[87]

Analogs that contained only β^3-amino acid substitutions in the hydrophilic face (Figure 21b) exhibited a similar tendency, a slight increase 9-18 % in β-sheet content. The hydrophobic nature of the non-matching substitutions resulted in higher slopes for β-sheet increase (Figure 21c), however, the lack of structural melting pointed to missing cooperative folding.

It has been shown that anginex related β-sheets tend to self-associate to higher ordered β-sandwich structures as a further stabilization of the fold. In order to investigate self-association, pulsed field-gradient spin echo (PFGSE) Diffusion Ordered Spectroscopy (DOSY) NMR measurements were carried out. The calculated hydrodynamic radius based on the measured diffusion coefficients for anginex-Gly was 15.6 Å at 500 μM at 37 °C (Figure 22a), which indicated the formation of tetramers.

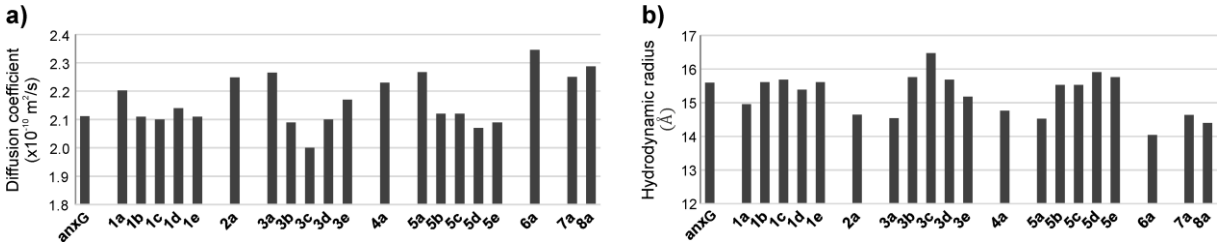

Figure 22. a) Diffusion coefficients measured by NMR and **b)** calculated hydrodynamic radii for anginex-Gly and analogs.

The hydrodynamic radii of the foldamers were in the range of 14.0 to 16.4 Å (Figure 22b). The CD and NMR data indicated increased disorder for all of the analogs, which had a radius increasing effect without oligomerization.[163] There was no significant correlation with the substitution positions, only a few tendencies could be observed. Most of the analogs that contained only β^3-amino acid substitutions (**1a**-**8a**) displayed slightly lower hydrodynamic radii, which could be explained by diminished tendency to aggregation which counteracted the increased dimensions caused by unfolded chains. Analogs with higher hydrodynamic radii may comprise of partially unfolded regions along with retained ability of self-association, which was observed mainly with analogs containing cyclic amino acid residues (patterns **c**, **d** and **e**). **3c** exhibited the highest radius that was one of the most unstructured analogs, which might be due to the large unfolded population.

4.2. Substitution effects on biological activity

4.2.1. Interaction with gal-1

Our goal was to investigate whether the analogs having β^3-amino acid substitutions maintain their affinity toward gal-1 the target protein of anginex. Anginex – gal-1 interactions were characterized previously via surface plasmon resonance[17], fluorescence anisotropy[135] but the solution state interaction of this complex was not available. In order to be able to test the interaction with the target protein via ITC[164] the measurement conditions had to be optimized using the parent sequence. The experiments included a mutant V5D gal-1 with reduced tendency for dimerization.

Optimization of experimental conditions

Solubility and aggregation of anginex-Gly is affected by pH, temperature and the choice of buffer, therefore 15 μM protein concentration was used on the cell in order to reduce the chance of aggregation. Gal-1 is prone to form dimers with a dissociation constant of 1-7 μM,[132-133] therefore the monomer-dimer interconversion of gal-1 might also contribute to the detected net enthalpy changes. In order to rule this out, experiment was performed with a V5D mutant gal-1 with decreased dimerization tendency, by having a Val to Asp mutation in the dimerization interface.[165] Titrations in Tris buffer with 15 μM protein concentration in the cell at pH 7.4, 35°C yielded well-detectable signals for both proteins. Further experiments were carried out using these conditions.

Determination of binding affinity

The titration of wt gal-1 revealed a two-stage interaction: well detectable exothermic peaks were observed suggesting high-affinity binding and second endothermic peaks were observed with low enthalpy changes (Figure 23a). The data was fitted using the two independent binding sites model which resulted in the following values for the first step: $n_1 = 0.23 \pm 0.02$, $\Delta H_{b1} = -3.4 \pm 0.4$ kcal/mol and an apparent dissociation constant $K_{D1} = 7 \pm 3$ nM. The second step resulted in $n_2 = 0.95 \pm 0.15$, $\Delta H_{b2} = 0.3 \pm 0.1$ kcal/mol and $K_{D2} = 220 \pm 77$ nM (Table 3.) The stoichiometry of the first step suggested 4:1 gal-1 – anginex-Gly interaction, whereas the second step corresponded to 1:1 binding. The total stoichiometry of 1.25 indicated that the two interactions occurred parallel and there was no competition between them. Titration of V5D resulted in similar stoichiometry and affinity, the binding enthalpy for the second step was significantly higher (Figure 23b, Table 3.)

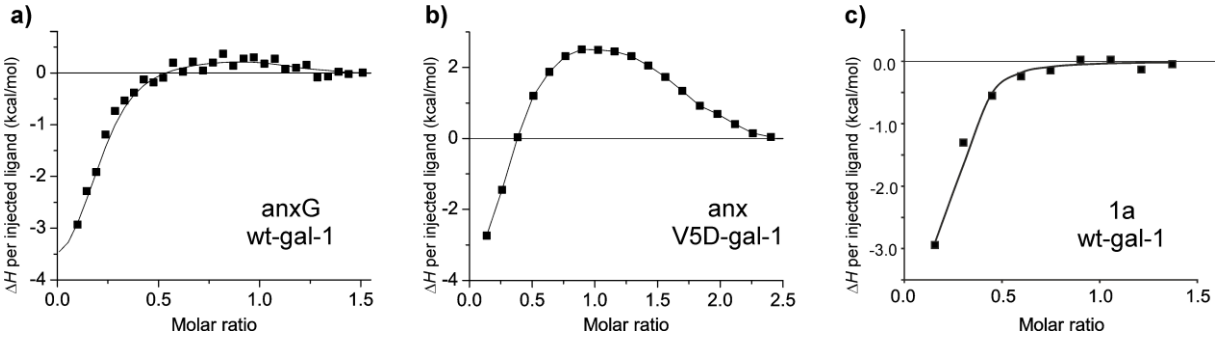

Figure 23. ITC enthalpograms of **a)** anginex-Gly (anxG) titrated to wt-gal-1 **b)** anginex-Gly titrated to V5D gal-1 and **c) 1a** titrated to wt-gal-1.

Non-covalent bond complementarity in a protein-ligand complex results in favorable enthalpic contribution upon complex formation, which gives negative Δ*H* values in an ITC experiment.[166] The favorable enthalpy of the first step suggested good non-covalent bond complementarity, whereas the endothermic second step pointed to higher contribution of hydrophobic interactions and resulted in an entropically driven binding. These results suggested that the high affinity binding step involved structural features which were present both in the wt and the mutated V5D gal-1 and was not affected by the dimerization equilibrium of the protein.

Table 3. Summary of the thermodynamic data of anginex-Gly gal-1 interaction.

	n_1	K_{D1} (nM)	ΔH_{b1} (kcal/mol)	ΔS_1 (cal/mol/K)	n_2	K_{D2} (nM)	ΔH_{b2} (kcal/mol)	ΔS_2 (cal/mol/K)
wt gal-1	0.23±0.02	7±3	-3.4±0.4	26.5	0.95±0.15	220±77	0.3±0.1	31.5
V5D gal-1	0.28±0.01	21±1	-4.6±0.7	23.0	1.10±0.03	387±18	3.3±0.2	40.0
1a	0.22±0.01	188±4	-3.5±0.5	17.5	-	-	-	-

ITC titrations were performed with analogs having β^3-amino acid substitutions in order to test the effect of structural change with remained pharmacophore side-chains. Binding was detected only with **1a** that exhibited similar stoichiometry but decreased affinity (Figure 23c, Table 3) compared to that of the parent peptide and the second step was not observed. The inability of the analogs to bind to the target protein could be explained by the misalignment of the pharmacophore anchor points caused by the extra methylene group in the backbone or the disruption of the secondary structure, which eventually led to decreased affinity.

4.2.2. Interaction with membranes

The complexity of the mechanism of action of anginex led us to investigate other aspects of biological activity by *in vitro* cell-based assay and membrane interactions. *In vitro* assays

and membrane leakage experiments were performed and evaluated by Ildikó Makra (PhD School in Biology, University of Szeged), Lymphocyte Signal Transduction Group led by Dr. Éva Monostori, in the Biological Research Centre; and these results are part of her PhD dissertation. Here I provide only a brief summary of the biological activity in order to give a thorough picture of the substitution effects.

Table 4. IC_{50} values for anginex analogs based on MTT assay for **1a-8a** and FACS analysis for analogs with b-e patterns.

	IC_{50} μM		**IC_{50} μM**		**IC_{50} μM**
1a	68.8	**3b**	40.4	**5c**	138.5
1b	35.7	**3c**	n.i.	**5d**	136.4
1c	46.5	**3d**	30.7	**5e**	126.4
1d	35.6	**3e**	n.i.	**6a**	28.3
1e	46.4	**4a**	n.i.	**7a**	n.i.
2a	20.7	**5a**	71.6	**8a**	n.i.
3a	117.4	**5b**	56.4	**anxG**	52.2

A number of analogs displayed antiproliferative effects on bEND.3 mouse endothelial cell line, with close affinity to the parent peptide (Table 4). FACS experiments with analogs that have substitutions in the hydrophobic region revealed membrane disruption as the main cause of cytotoxicity, which had been shown previously for anginex.[16]

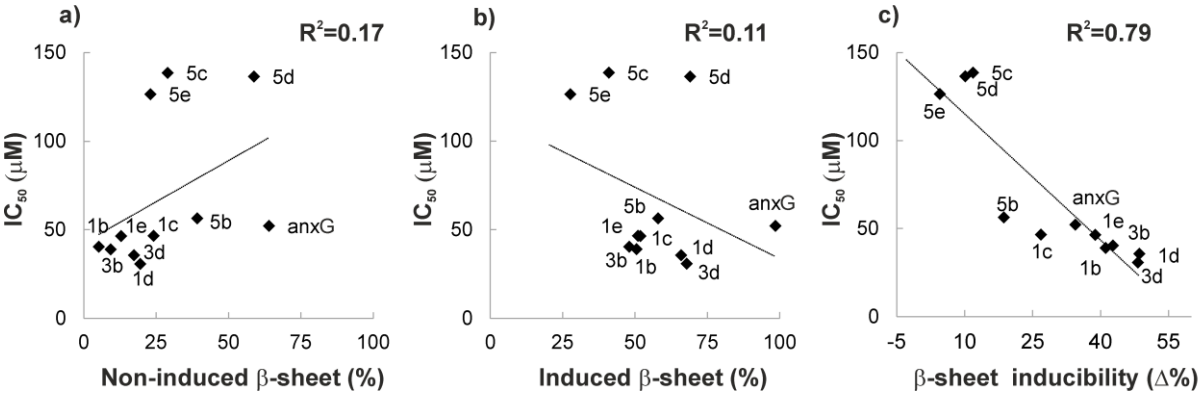

Figure 24. Correlation between IC_{50} of analogs with substitutions in the hydrophobic face, measured by FACS analysis and β-sheet structure. IC_{50} was plotted against β-sheet content % calculated by using the CCA+ software. Correlations are illustrated with **a)** the uninduced β-sheet content; **b)** the β-sheet content induced by DPC; and **c)** the β-sheet inducibility (the difference between the induced and uninduced β-sheet contents, expressed in Δ%).

Investigations of structure-activity relationship revealed no correlation between the initial or the induced β-sheet content (Figure 24.). High correlation was found between inducibility and cell viability, which suggested that the conversion from random coil to the β-sheet during

interaction with the membrane was the key for biological activity in case of substitutions in the hydrophobic positions and decreasing the conformational diversity was detrimental to *in vitro* bioactivity. This was further supported by membrane leakage experiments with artificial micelles mimicking neutral and negatively charged membranes. Treatment of these micelles with selected peptides revealed specificity toward negatively charged membranes, which might contribute to selectivity. These results highlighted that the pre-formed globally amphiphilic structure was not prerequisite for the interaction as was shown with membrane interacting foldamer helices[93], with the extension that in our case the extent of β-sheet inducibility was crucial for biological activity.

4.3. Conclusions

Through a systematic α → β substitution approach 20 α/β-peptide analogs were designed and synthesized based on the antiparallel β-sheet forming anginex. This study was the first to address the effects of β-amino acid substitutions in a system larger than a minimal hairpin. The folding behavior of the analogs were investigated from different aspects, regarding turn initiation, hydrogen-bond pattern and local conformational preferences as well as the secondary structure propensity and overall folding by means of NMR and CD spectroscopy.

Structural investigations revealed that the turn rigidity of the parent peptide decreased and depended on the substitution position. Substitutions closer to the turns caused more flexible turn segment, which might contribute to the overall stability of the β-sheets. Conformational preference of the substituted amino acids revealed that residues with branched side-chains next to C^{β} (β^3*h*Val and β^3*h*Ile) were able to obtain *gauche* conformation that could fit to the hydrogen bonding pattern of the β-sheet, and suggested that the use of constrained residues with preorganized conformation was advantageous. This indicated that the destructuring effect was not primarily due to the impaired conformation or disrupted hydrogen-bond pattern.

Secondary chemical shift analysis was found to be a useful tool to analyze the tendencies of transient structure formation at the amino acid level. All analogs exhibited lower β-sheet folding tendency, which primarily depended on the substitution position: substitutions in the core exhibited higher destructuring effects than those at the edge. β^3-Amino acid substitutions caused an undesired helix formation in the more flexible strand of anginex, whereas the use of constrained residues diminished this tendency, which suggested that the monomeric unit had to be chosen carefully as it could alter the conformational preference of an entire chain with higher flexibility.

CD spectroscopy revealed that the diverse conformational behavior of the parent peptide could be maintained and tuned by the substitutions. After provision of membrane mimicking environment the β-sheet fold could be induced to different extents. Highest inducibility was shown by the peripheral substitutions, core substitutions were not tolerated. Hydrophobic forces that stabilize the β-sheet fold were scaled down as revealed by temperature dependent measurements. Only those analogs could maintain the biomimetic behavior that had similar solvent exposed surface as the original amino acids. These observations pointed out that the side-chain compatibility with the hydrophobic core was the most important stabilizing effect in α/β-peptidic sequences.

The retained inducible β-sheet formation was promising for biological activity. ITC studies showed that only one analog could retain its activity toward the target protein gal-1. *In vitro* activity, however, resulted in close inhibitory potential to the parent peptide for several analogs, which pointed toward more complex mechanism of action and higher contribution of membrane interactions to the biological activity. The finding that β-sheet inducibility is required for *in vitro* bioactivity highlighted the importance of maintaining the diverse structural features.

With this design strategy we were able to mimic the diverse conformational behavior of the β-sheet of anginex, which might be extended to other hydrophobically stabilized α/β-peptides, with the following considerations: i) utilization of conformationally constrained residues in a more flexible chain is advantageous for strand formation ii) replacements to hydrophobic amino acids with branched side-chains or constrained amino acids fit better to the hydrogen bond pattern, iii) substitutions in the core region should be avoided, peripheral and close replacements to the turn are more tolerable iv) turn instability caused by close substitutions can be compensated by creation of a hydrophobic cluster near to the turn, which results in increased inducibility.

By understanding the effects of β-amino acid substitutions in a hydrophobically stabilized β-sheet revealed an excellent tool to control the β-sheet forming propensity. This may result in valuable bioactive α/β-peptides or can be used as a tool to investigate structure-function relationships. With the combination of the established rules, β-sheet forming α/β-peptides could be constructed having higher β-amino acid content and therefore increased proteolytic stability. The ability to control the β-sheet formation with the help of α/β-peptides may also help us to avoid the high aggregational tendency of β-sheets and result in pharmacologically advantageous compounds.

5. Summary

1. 20 β-amino acid containing α/β-peptides were designed in order to investigate the rules of β-sheet folding in an α/β-foldameric system.
   1.1. The design strategy involved systematic substitutions with homologous β^3-amino acids and with conformationally constrained amino acids.
   1.2. The designed peptides were successfully synthesized after optimization of synthesis conditions in order to avoid aspartimide related byproduct formation.
2. NMR spectroscopic studies revealed diverse behavior regarding turn initiation and local conformational preferences:
   2.1. The chemical shifts of all analogs could be successfully assigned after optimization of the measurement conditions.
   2.2. β-amino acid substitutions close to the turn segment increased its flexibility.
   2.3. Local conformational preferences of the β^3-amino acids revealed that they were able to adopt the desired conformation that fitted to the hydrogen-bonding pattern of the β-sheet.
3. Secondary chemical shift analysis and SSP score calculation was useful to evaluate the secondary structure forming propensity at an amino acid level:
   3.1. H^α and C^α chemical shifts were the most informative about secondary structure changes and NH chemical shifts were the least affected by the different substitutions.
   3.2. β^3-Amino acid substitutions induced an undesired helix formation in the more flexible strand of the peptide while the use of constrained residues completely inhibited this tendency.
   3.3. Substitutions were the most tolerable close to the turn or in the peripheral regions.
   3.4. After addition of the membrane-mimicking phospholipid the ^1H NMR spectra of the compounds exhibited β-sheet folding, however signal assignment was prevented due to signal intensity loss and line-broadening.
4. Overall and temperature dependent folding of the foldamers were analyzed by CD:
   4.1. Without induction the foldamers displayed high random coil content, after provision of the membrane-mimicking DPC β-sheet folding was apparent for most of the analogs.
   4.2. Quantitative estimation of the secondary structure content revealed different extent of β-sheet content and inducibility, showing the preference of substitutions close to the turn and peripheral regions, which were in line with the NMR results.

4.3. Temperature dependent CD measurement revealed that the stabilizing hydrophobic forces were scaled down, which contributed mostly to the destructuring effect of β-amino acids. The presence and stabilizing factor of the hydrophobic forces were more pronounced at positions where the turn stability decreased.

4.4. Substitutions did not result in increased aggregation or self-association, the determined hydrodynamic radii were close to the parent sequence.

5. Investigation of the biological activity was carried out by ITC and in vitro experiments

5.1. Gal-1 anginex-Gly interaction was successfully characterized by ITC, which revealed 1:4 stoichiometry and high affinity

5.2. Most of the substitutions were detrimental to gal-1 binding, which might originate from the changed position of pharmacophore points or decreased folding.

5.3. A number of analogs displayed *in vitro* activity close to the parent sequence, which were in correlation with the β-sheet inducibility.

Acknowledgements

This work was carried out in the Institute of Pharmaceutical Chemistry over the years 2011-2014 and in the Institute of Pharmaceutical Analysis, University of Szeged in the years 2014 and 2015.

I would like to express my deep gratitude to my supervisor Prof. Dr. Tamás Martinek, Head of the Institute of Pharmaceutical Analysis for his guidance to complete this work, his inspiring ideas and constructive suggestions.

I owe my thanks to Dr. Edit Wéber and Dr. Anasztázia Hetényi for performing the NMR measurements and helping me when any difficulties arose.

I express sincere thanks to the members of the Monostori group at the Laboratory of Lymphocyte and Signal Transduction, Biological Research Centre, especially to Ildikó Makra and Dr. Éva Kriston-Pál for performing the *in vitro* assays and to Prof. Dr. Éva Monostori for her constructive support. I also thank Balázs Váczi and Lea Végh and Vilmos Tubak for the cloning and expression of galectin-1.

I am grateful to Dr. István Mándity for providing insights to peptide synthetic methods and to Prof. Dr. Ferenc Fülöp head of Institute of Pharmaceutical Chemistry for providing me with the possibility to carry out part of my work in this institute.

I owe my thanks to Dr. Erzsébet Kopházi-Molnár and Dr. László Molnár for revising the English language of my thesis.

I am grateful to all my colleagues in the Institute of Pharmaceutical Analysis and Pharmaceutical Chemistry for their help and useful advice.

I wish to express my warmest thanks to my family and friends for their encouragement and understanding during my PhD studies.

References

1. A. M. Watkins and P. S. Arora, *ACS Chem. Biol.*, **2014**, *9*, 1747-1754.
2. E. J. Dufourc, S. Buchoux, J. Toupe, M. A. Sani, F. Jean-Francois, L. Khemtemourian, A. Grelard, C. Loudet-Courreges, M. Laguerre, J. Elezgaray, B. Desbat and B. Odaert, *Curr. Protein Pept. Sci.*, **2012**, *13*, 620-631.
3. C. Cabrele, T. A. Martinek, O. Reiser and Ł. Berlicki, *J. Med. Chem.*, **2014**, *57*, 9718-9739.
4. H. M. Werner and W. S. Horne, *Curr. Opin. Chem. Biol.*, **2015**, *28*, 75-82.
5. I. M. Mándity and F. Fülöp, *Expert Opin. Drug Discovery*, **2015**, *10*, 1163-1177.
6. J. S. Nowick, K. S. Lam, T. V. Khasanova, W. E. Kemnitzer, S. Maitra, H. T. Mee and R. Liu, *J. Am. Chem. Soc.*, **2002**, *124*, 4972-4973.
7. J. S. Nowick, *Acc. Chem. Res.*, **2008**, *41*, 1319-1330.
8. C. Liu, M. R. Sawaya, P.-N. Cheng, J. Zheng, J. S. Nowick and D. Eisenberg, *J. Am. Chem. Soc.*, **2011**, *133*, 6736-6744.
9. O. Khakshoor and J. S. Nowick, *Curr. Opin. Chem. Biol.*, **2008**, *12*, 722-729.
10. P. N. Cheng, C. Liu, M. Zhao, D. Eisenberg and J. S. Nowick, *Nat. Chem.*, **2012**, *4*, 927-933.
11. R. Spencer, K. H. Chen, G. Manuel and J. S. Nowick, *Eur. J. Org. Chem.*, **2013**, *2013*, 3523-3528.
12. R. J. Woods, J. O. Brower, E. Castellanos, M. Hashemzadeh, O. Khakshoor, W. A. Russu and J. S. Nowick, *J. Am. Chem. Soc.*, **2007**, *129*, 2548-2558.
13. A. Griffioen, D. van der Schaft, A. Barendsz-Janson, A. Cox, B. H. Struijker, H. Hillen and K. Mayo, *Biochem. J*, **2001**, *354*, 233-242.
14. D. W. van der Schaft, R. P. Dings, Q. G. de Lussanet, L. I. van Eijk, A. W. Nap, R. G. Beets-Tan, J. C. Bouma-Ter Steege, J. Wagstaff, K. H. Mayo and A. W. Griffioen, *FASEB J.*, **2002**, *16*, 1991-1993.
15. J. B. Wang, M. D. Wang, E. X. Li and D. F. Dong, *Peptides*, **2012**, *38*, 457-462.
16. J. Pilch, C. M. Franzin, L. M. Knowles, F. J. Ferrer, F. M. Marassi and E. Ruoslahti, *J. Mol. Biol.*, **2006**, *356*, 876-885.
17. V. L. Thijssen, R. Postel, R. J. Brandwijk, R. P. Dings, I. Nesmelova, S. Satijn, N. Verhofstad, Y. Nakabeppu, L. G. Baum, J. Bakkers, K. H. Mayo, F. Poirier and A. W. Griffioen, *Proc. Natl. Acad. Sci. U. S. A.*, **2006**, *103*, 15975-15980.
18. K. H. Mayo, E. Ilyina and H. Park, *Protein Sci.*, **1996**, *5*, 1301-1315.
19. J. F. Espinosa, F. A. Syud and S. H. Gellman, *Protein Sci.*, **2002**, *11*, 1492-1505.
20. T. Kortemme, M. Ramírez-Alvarado and L. Serrano, *Science*, **1998**, *281*, 253-256.
21. E. D. Alba, J. Santoro, M. Rico and M. A. Jiménez, *Protein Sci.*, **1999**, *8*, 854-865.
22. H. E. Stanger and S. H. Gellman, *J. Am. Chem. Soc.*, **1998**, *120*, 4236-4237.
23. A. M. Fernandez-Escamilla, S. Ventura, L. Serrano and M. A. Jimenez, *Protein Sci.*, **2006**, *15*, 2278-2289.
24. H. L. Schenck and S. H. Gellman, *J. Am. Chem. Soc.*, **1998**, *120*, 4869-4870.
25. G. A. Lengyel, R. C. Frank and W. S. Horne, *J. Am. Chem. Soc.*, **2011**, *133*, 4246-4249.
26. G. A. Lengyel and W. S. Horne, *J. Am. Chem. Soc.*, **2012**, *134*, 15906-15913.
27. Z. E. Reinert, G. A. Lengyel and W. S. Horne, *J. Am. Chem. Soc.*, **2013**, *135*, 12528-12531.
28. S. Hecht and I. Huc, *Foldamers : Structure, Properties, and Applications*, Wiley-VCH, Weinheim, 2007.
29. R. W. Cheloha, J. A. Sullivan, T. Wang, J. M. Sand, J. Sidney, A. Sette, M. E. Cook, M. Suresh and S. H. Gellman, *ACS Chem. Biol.*, **2015**, *10*, 844-854.
30. J. Frackenpohl, P. I. Arvidsson, J. V. Schreiber and D. Seebach, *ChemBioChem*, **2001**, *2*, 445-455.
31. H. N. Gopi, G. Ravindra, P. P. Pal, P. Pattanaik, H. Balaram and P. Balaram, *FEBS Lett.*, **2003**, *535*, 175-178.
32. H. S. Haase, K. J. Peterson-Kaufman, S. K. Lan Levengood, J. W. Checco, W. L. Murphy and S. H. Gellman, *J. Am. Chem. Soc.*, **2012**, *134*, 7652-7655.
33. J. D. Sadowsky, J. K. Murray, Y. Tomita and S. H. Gellman, *ChemBioChem*, **2007**, *8*, 903-916.
34. D. F. Hook, P. Bindschädler, Y. R. Mahajan, R. Šebesta, P. Kast and D. Seebach, *Chem. Biodiversity*, **2005**, *2*, 591-632.
35. D. Seebach, S. Abele, J. V. Schreiber, B. Martinoni, A. K. Nussbaum, H. Schild, H. Schulz, H. Hennecke, R. Woessner and F. Bitsch, *Chimia*, **1998**, *52*, 734-739.

36. H. Wiegand, B. Wirz, A. Schweitzer, G. P. Camenisch, M. I. Rodriguez Perez, G. Gross, R. Woessner, R. Voges, P. I. Arvidsson and J. Frackenpohl, *Biopharm. Drug Dispos.*, **2002**, *23*, 251-262.
37. D. Seebach, A. K. Beck and D. J. Bierbaum, *Chem. Biodiversity*, **2004**, *1*, 1111-1239.
38. F. Fülöp, T. A. Martinek and G. K. Tóth, *Chem. Soc. Rev.*, **2006**, *35*, 323-334.
39. W. S. Horne and S. H. Gellman, *Accounts of chemical research*, **2008**, *41*, 1399-1408.
40. L. K. Pilsl and O. Reiser, *Amino Acids*, **2011**, *41*, 709-718.
41. T. A. Martinek and F. Fülöp, *Chem. Soc. Rev.*, **2012**, *41*, 687-702.
42. D. Seebach and J. L. Matthews, *Chem. Commun. (Cambridge, U. K.)*, **1997**, 2015-2022.
43. É. Szolnoki, A. Hetényi, T. A. Martinek, Z. Szakonyi and F. Fülöp, *Org. Biomol. Chem.*, **2012**, *10*, 255-259.
44. É. Szolnoki, A. Hetényi, I. M. Mándity, F. Fülöp and T. A. Martinek, *Eur. J. Org. Chem.*, **2013**, *2013*, 3555-3559.
45. Ł. Berlicki, L. Pilsl, E. Wéber, I. M. Mándity, C. Cabrele, T. A. Martinek, F. Fülöp and O. Reiser, *Angew. Chem., Int. Ed.*, **2012**, *51*, 2208-2212.
46. S. Chandrasekhar, B. N. Babu, A. Prabhakar, A. Sudhakar, M. S. Reddy, M. U. Kiran and B. Jagadeesh, *Chem Commun (Camb)*, **2006**, 1548-1550.
47. T. A. Martinek, A. Hetenyi, L. Fulop, I. M. Mandity, G. K. Toth, I. Dekany and F. Fulop, *Angew. Chem., Int. Ed. Engl.*, **2006**, *45*, 2396-2400.
48. J. L. Price, W. S. Horne and S. H. Gellman, *J. Am. Chem. Soc.*, **2010**, *132*, 12378-12387.
49. Z. E. Reinert and W. S. Horne, *Org. Biomol. Chem.*, **2014**, *12*, 8796-8802.
50. I. M. Mándity, E. Wéber, T. A. Martinek, G. Olajos, G. K. Tóth, E. Vass and F. Fülöp, *Angew. Chem.*, **2009**, *121*, 2205-2209.
51. B. F. Fisher, L. Guo, B. S. Dolinar, I. A. Guzei and S. H. Gellman, *J. Am. Chem. Soc.*, **2015**.
52. M. W. Giuliano, S. J. Maynard, A. M. Almeida, L. Guo, I. A. Guzei, L. C. Spencer and S. H. Gellman, *J. Am. Chem. Soc.*, **2014**, *136*, 15046-15053.
53. W. S. Horne, *Expert Opin. Drug Discovery*, **2011**, *6*, 1247-1262.
54. W. S. Horne, M. D. Boersma, M. A. Windsor and S. H. Gellman, *Angew. Chem., Int. Ed.*, **2008**, *47*, 2853-2856.
55. L. Fulop, I. M. Mandity, G. Juhasz, V. Szegedi, A. Hetenyi, E. Weber, Z. Bozso, D. Simon, M. Benko, Z. Kiraly and T. A. Martinek, *PLoS One*, **2012**, *7*, e39485.
56. J. A. Kritzer, N. W. Luedtke, E. A. Harker and A. Schepartz, *J. Am. Chem. Soc.*, **2005**, *127*, 14584-14585.
57. J. K. Murray, B. Farooqi, J. D. Sadowsky, M. Scalf, W. A. Freund, L. M. Smith, J. Chen and S. H. Gellman, *J. Am. Chem. Soc.*, **2005**, *127*, 13271-13280.
58. J. A. Kritzer, J. D. Lear, M. E. Hodsdon and A. Schepartz, *J. Am. Chem. Soc.*, **2004**, *126*, 9468-9469.
59. J. A. Kritzer, J. Tirado-Rives, S. A. Hart, J. D. Lear, W. L. Jorgensen and A. Schepartz, *J. Am. Chem. Soc.*, **2005**, *127*, 167-178.
60. E. A. Harker and A. Schepartz, *ChemBioChem*, **2009**, *10*, 990-993.
61. J. D. Sadowsky, M. A. Schmitt, H.-S. Lee, N. Umezawa, S. Wang, Y. Tomita and S. H. Gellman, *J. Am. Chem. Soc.*, **2005**, *127*, 11966-11968.
62. E. F. Lee, J. D. Sadowsky, B. J. Smith, P. E. Czabotar, K. J. Peterson-Kaufman, P. M. Colman, S. H. Gellman and W. D. Fairlie, *Angew. Chem.*, **2009**, *121*, 4382-4386.
63. K. J. Peterson-Kaufman, H. S. Haase, M. D. Boersma, E. F. Lee, W. D. Fairlie and S. H. Gellman, *ACS Chem. Biol.*, **2015**, *10*, 1667-1675.
64. S. J. Shandler, I. V. Korendovych, D. T. Moore, K. B. Smith-Dupont, C. N. Streu, R. I. Litvinov, P. C. Billings, F. Gai, J. S. Bennett and W. F. DeGrado, *J. Am. Chem. Soc.*, **2011**, *133*, 12378-12381.
65. Y. Imamura, N. Watanabe, N. Umezawa, T. Iwatsubo, N. Kato, T. Tomita and T. Higuchi, *J. Am. Chem. Soc.*, **2009**, *131*, 7353-7359.
66. Y. Imamura, N. Umezawa, S. Osawa, N. Shimada, T. Higo, S. Yokoshima, T. Fukuyama, T. Iwatsubo, N. Kato, T. Tomita and T. Higuchi, *J. Med. Chem.*, **2013**, *56*, 1443-1454.
67. O. M. Stephens, S. Kim, B. D. Welch, M. E. Hodsdon, M. S. Kay and A. Schepartz, *J. Am. Chem. Soc.*, **2005**, *127*, 13126-13127.

68. A. D. Bautista, O. M. Stephens, L. Wang, R. A. Domaoal, K. S. Anderson and A. Schepartz, *Bioorg. Med. Chem. Lett.*, **2009**, *19*, 3736-3738.
69. L. M. Johnson, D. E. Mortenson, H. G. Yun, W. S. Horne, T. J. Ketas, M. Lu, J. P. Moore and S. H. Gellman, *J. Am. Chem. Soc.*, **2012**, *134*, 7317-7320.
70. L. M. Johnson, W. S. Horne and S. H. Gellman, *J. Am. Chem. Soc*, **2011**, *133*, 10038-10041.
71. H. S. Haase, K. J. Peterson-Kaufman, S. K. Lan Levengood, J. W. Checco, W. L. Murphy and S. H. Gellman, *J. Am. Chem. Soc*, **2012**, *134*, 7652-7655.
72. J. W. Checco, D. F. Kreitler, N. C. Thomas, D. G. Belair, N. J. Rettko, W. L. Murphy, K. T. Forest and S. H. Gellman, *Proc. Natl. Acad. Sci. U. S. A.*, **2015**, *112*, 4552-4557.
73. R. W. Cheloha, A. Maeda, T. Dean, T. J. Gardella and S. H. Gellman, *Nat. Biotechnol.*, **2014**, *32*, 653-655.
74. E. V. Denton, C. J. Craig, R. L. Pongratz, J. S. Appelbaum, A. E. Doerner, A. Narayanan, G. I. Shulman, G. W. Cline and A. Schepartz, *Org. Lett.*, **2013**, *15*, 5318-5321.
75. V. Azzarito, K. Long, N. S. Murphy and A. J. Wilson, *Nat Chem*, **2013**, *5*, 161-173.
76. S. A. Hart, A. B. F. Bahadoor, E. E. Matthews, X. J. Qiu and A. Schepartz, *J. Am. Chem. Soc.*, **2003**, *125*, 4022-4023.
77. W. S. Horne, J. L. Price and S. H. Gellman, *Proc. Natl. Acad. Sci. U. S. A.*, **2008**, *105*, 9151-9156.
78. W. S. Horne and S. H. Gellman, *Acc. Chem. Res.*, **2008**, *41*, 1399-1408.
79. E. Torres, E. Gorrea, K. K. Burusco, E. Da Silva, P. Nolis, F. Rua, S. Boussert, I. Diez-Perez, S. Dannenberg, S. Izquierdo, E. Giralt, C. Jaime, V. Branchadell and R. M. Ortuno, *Org. Biomol. Chem.*, **2010**, *8*, 564-575.
80. S. Chandrasekhar, A. Sudhakar, M. U. Kiran, B. N. Babu and B. Jagadeesh, *Tetrahedron Lett.*, **2008**, *49*, 7368-7371.
81. Y. J. Chung, B. R. Huck, L. A. Christianson, H. E. Stanger, S. Krauthauser, D. R. Powell and S. H. Gellman, *J. Am. Chem. Soc.*, **2001**, *123*, 5851-5851.
82. D. Seebach, S. Abele, K. Gademann and B. Jaun, *Angew. Chem., Int. Ed.*, **1999**, *38*, 1595-1597.
83. C. R. Jones, M. K. N. Qureshi, F. R. Truscott, S. T. D. Hsu, A. J. Morrison and M. D. Smith, *Angew. Chem., Int. Ed.*, **2008**, *47*, 7099-7102.
84. M. Khurram, N. Qureshi and M. D. Smith, *Chem. Commun. (Cambridge, U. K.)*, **2006**, 5006-5008.
85. R. Sonti, H. N. Gopi, U. Muddegowda, S. Ragothama and P. Balaram, *Chemistry*, **2013**, *19*, 5955-5965.
86. G. L. Montalvo, Y. Zhang, T. M. Young, M. J. Costanzo, K. B. Freeman, J. Wang, D. J. Clements, E. Magavern, R. W. Kavash and R. W. Scott, *ACS Chem. Biol.*, **2014**, *9*, 967-975.
87. G. Olajos, A. Hetényi, E. Wéber, L. J. Németh, Z. Szakonyi, F. Fülöp and T. A. Martinek, *Chem. – Eur. J.*, **2015**, *21*, 6173-6180.
88. C. Douat, C. Aisenbrey, S. Antunes, M. Decossas, O. Lambert, B. Bechinger, A. Kichler and G. Guichard, *Angew. Chem., Int. Ed.*, **2015**, *54*, 11133-11137.
89. T. L. Raguse, E. A. Porter, B. Weisblum and S. H. Gellman, *J. Am. Chem. Soc.*, **2002**, *124*, 12774-12785.
90. D. Liu and W. F. DeGrado, *J. Am. Chem. Soc.*, **2001**, *123*, 7553-7559.
91. Y. Hamuro, J. P. Schneider and W. F. DeGrado, *J. Am. Chem. Soc.*, **1999**, *121*, 12200-12201.
92. E. A. Porter, X. Wang, H.-S. Lee, B. Weisblum and S. H. Gellman, *Nature*, **2000**, *404*, 565-565.
93. M. A. Schmitt, B. Weisblum and S. H. Gellman, *J. Am. Chem. Soc.*, **2007**, *129*, 417-428.
94. M. Ramírez-Alvarado, T. Kortemme, F. J. Blanco and L. Serrano, *Bioorg. Med. Chem.*, **1999**, *7*, 93-103.
95. F. A. Syud, H. E. Stanger and S. H. Gellman, *J. Am. Chem. Soc.*, **2001**, *123*, 8667-8677.
96. S. H. Gellman, *Curr. Opin. Chem. Biol.*, **1998**, *2*, 717-725.
97. Y. Yan and B. W. Erickson, *Protein Sci.*, **1994**, *3*, 1069-1073.
98. A. Lim, A. M. Makhov, M. J. Saderholm, J. D. Griffith and B. W. Erickson, *Biochem. Biophys. Res. Commun.*, **1999**, *264*, 498-504.
99. A. Lim, M. J. Saderholm, A. M. Makhov, M. Kroll, Y. Yan, L. Perera, J. D. Griffith and B. W. Erickson, *Protein Sci.*, **1998**, *7*, 1545-1554.
100. R. Guerois and M. López de la Paz, *Protein Design : Methods and Applications*, Humana Press, Totowa, N.J., 2006.
101. E. d. Alba, M. A. Jiménez, M. Rico and J. L. Nieto, *Folding and Design*, **1996**, *1*, 133-144.

102. K. L. Constantine, L. Mueller, N. H. Andersen, H. Tong, C. F. Wandler, M. S. Friedrichs and R. E. Bruccoleri, *J. Am. Chem. Soc.*, **1995**, *117*, 10841-10854.
103. M. Ramirez-Alvarado, F. J. Blanco and L. Serrano, *Nat. Struct. Mol. Biol.*, **1996**, *3*, 604-612.
104. G. Colombo, G. M. De Mori and D. Roccatano, *Protein Sci.*, **2003**, *12*, 538-550.
105. F. A. Syud, H. E. Stanger, H. S. Mortell, J. F. Espinosa, J. D. Fisk, C. G. Fry and S. H. Gellman, *J. Mol. Biol.*, **2003**, *326*, 553-568.
106. H. E. Stanger, F. A. Syud, J. F. Espinosa, I. Giriat, T. Muir and S. H. Gellman, *Proc. Natl. Acad. Sci. U. S. A.*, **2001**, *98*, 12015-12020.
107. K. H. Mayo and E. Ilyina, *Protein Sci.*, **1998**, *7*, 358-368.
108. K. H. Mayo, J. Haseman, E. Ilyina and B. Gray, *Biochim. Biophys. Acta*, **1998**, *1425*, 81-92.
109. R. J. Brandwijk, I. Nesmelova, R. P. Dings, K. H. Mayo, V. L. Thijssen and A. W. Griffioen, *Biochem. Biophys. Res. Commun.*, **2005**, *333*, 1261-1268.
110. M. M. Arroyo and K. H. Mayo, *Biochim. Biophys. Acta*, **2007**, *1774*, 645-651.
111. R. P. M. Dings, D. W. J. van der Schaft, B. Hargittai, J. Haseman, A. W. Griffioen and K. H. Mayo, *Cancer Letters*, **2003**, *194*, 55-66.
112. R. P. Dings, J. R. Haseman and K. H. Mayo, *Biochem. J.*, **2008**, *414*, 143-150.
113. A. W. Griffioen, A. F. Barendsz-Janson, K. H. Mayo and H. F. Hillen, *J. Lab. Clin. Med.*, **1998**, *132*, 363-368.
114. A. Griffioen, *Angiogenesis*, **2006**, *9*, 155-170.
115. A. W. Griffioen, *Trends Cardiovasc Med*, **2007**, *17*, 171-176.
116. C. Ruegg, M. Hasmim, F. J. Lejeune and G. C. Alghisi, *Biochim. Biophys. Acta*, **2006**, *1765*, 155-177.
117. A. W. Griffioen, D. W. van der Schaft, A. F. Barendsz-Janson, A. Cox, H. A. Struijker Boudier, H. F. Hillen and K. H. Mayo, *Biochem. J.*, **2001**, *354*, 233-242.
118. R. J. Brandwijk, R. P. Dings, E. van der Linden, K. H. Mayo, V. L. Thijssen and A. W. Griffioen, *Biochem. Biophys. Res. Commun.*, **2006**, *349*, 1073-1078.
119. H. J. Mauceri, N. N. Hanna, M. A. Beckett, D. H. Gorski, M.-J. Staba, K. A. Stellato, K. Bigelow, R. Heimann, S. Gately and M. Dhanabal, *Nature*, **1998**, *394*, 287-291.
120. D. H. Gorski, H. J. Mauceri, R. M. Salloum, S. Gately, S. Hellman, M. A. Beckett, V. P. Sukhatme, G. A. Soff, D. W. Kufe and R. R. Weichselbaum, *Cancer Res.*, **1998**, *58*, 5686-5689.
121. B. A. Teicher, E. A. Sotomayor and Z. D. Huang, *Cancer Res.*, **1992**, *52*, 6702-6704.
122. U. Wilczynska, A. Kucharska, J. Szary and S. Szala, *Angiogenesis*, **2001**, *1*, 5-7.
123. R. P. Dings, M. Loren, H. Heun, E. McNiel, A. W. Griffioen, K. H. Mayo and R. J. Griffin, *Clin Cancer Res*, **2007**, *13*, 3395-3402.
124. R. P. Dings, Y. Yokoyama, S. Ramakrishnan, A. W. Griffioen and K. H. Mayo, *Cancer Res.*, **2003**, *63*, 382-385.
125. R. P. Dings, B. W. Williams, C. W. Song, A. W. Griffioen, K. H. Mayo and R. J. Griffin, *Int. J. Cancer*, **2005**, *115*, 312-319.
126. M. Yi, T. Sakai, R. Fässler and E. Ruoslahti, *Proc. Natl. Acad. Sci. U. S. A.*, **2003**, *100*, 11435-11438.
127. R. P. Dings, M. M. Arroyo, N. A. Lockwood, L. I. van Eijk, J. R. Haseman, A. W. Griffioen and K. H. Mayo, *Biochem. J.*, **2003**, *373*, 281-288.
128. K. H. Mayo, R. P. Dings, C. Flader, I. Nesmelova, B. Hargittai, D. W. van der Schaft, L. I. van Eijk, D. Walek, J. Haseman, T. R. Hoye and A. W. Griffioen, *J. Biol. Chem.*, **2003**, *278*, 45746-45752.
129. S. S. Hasan, G. M. Ashraf and N. Banu, *Cancer Lett*, **2007**, *253*, 25-33.
130. I. Camby, M. Le Mercier, F. Lefranc and R. Kiss, *Glycobiology*, **2006**, *16*, 137R-157R.
131. M. Salatino, D. O. Croci, G. A. Bianco, J. M. Ilarregui, M. A. Toscano and G. A. Rabinovich, *Expert Opin Biol Ther*, **2008**, *8*, 45-57.
132. E. Salomonsson, A. Larumbe, J. Tejler, E. Tullberg, H. Rydberg, A. Sundin, A. Khabut, T. Frejd, Y. D. Lobsanov, J. M. Rini, U. J. Nilsson and H. Leffler, *Biochemistry*, **2010**, *49*, 9518-9532.
133. M. Cho and R. D. Cummings, *J. Biol. Chem.*, **1995**, *270*, 5198-5206.
134. R. P. Dings, N. Kumar, M. C. Miller, M. L. Loren, H. Rangwala, T. R. Hoye and K. H. Mayo, *J. Pharmacol. Exp. Ther.*, **2012**, *344*, 589-599.

135. E. Salomonsson, V. L. Thijssen, A. W. Griffioen, U. J. Nilsson and H. Leffler, *J. Biol. Chem.*, **2011**, *286*, 13801-13804.
136. S. Ran, A. Downes and P. E. Thorpe, *Cancer Res.*, **2002**, *62*, 6132-6140.
137. I. M. Mandity, B. Olasz, S. B. Otvos and F. Fulop, *ChemSusChem*, **2014**, *7*, 3172-3176.
138. A. Perczel, K. Park and G. D. Fasman, *Anal. Biochem.*, **1992**, *203*, 83-93.
139. A. Perczel, M. Hollosi, G. Tusnady and G. D. Fasman, *Protein Eng.*, **1991**, *4*, 669-679.
140. A. Perczel, K. Park and G. D. Fasman, *Proteins*, **1992**, *13*, 57-69.
141. T. L. Hwang and A. J. Shaka, *J. Magn. Reson., Ser. A*, **1995**, *112*, 275-279.
142. B. Efron, *Biometrika*, **1981**, *68*, 589-599.
143. K. H. Mayo, D. W. van der Schaft and A. W. Griffioen, *Angiogenesis*, **2001**, *4*, 45-51.
144. S. Krauthäuser, L. A. Christianson, D. R. Powell and S. H. Gellman, *J. Am. Chem. Soc.*, **1997**, *119*, 11719-11720.
145. H. M. Yu, S. T. Chen and K. T. Wang, *J. Org. Chem.*, **1992**, *57*, 4781-4784.
146. S. A. Palasek, Z. J. Cox and J. M. Collins, *J. Pept. Sci.*, **2007**, *13*, 143-148.
147. M. Mergler, F. Dick, B. Sax, P. Weiler and T. Vorherr, *J. Pept. Sci.*, **2003**, *9*, 36-46.
148. D. Wishart, B. Sykes and F. Richards, *Biochemistry*, **1992**, *31*, 1647-1651.
149. T. L. Raguse, J. R. Lai and S. H. Gellman, *Helv. Chim. Acta*, **2002**, *85*, 4154-4164.
150. D. S. Wishart, B. D. Sykes and F. M. Richards, *Biochemistry*, **1992**, *31*, 1647-1651.
151. D. S. Wishart and A. M. Nip, *Biochem. Cell Biol.*, **1998**, *76*, 153-163.
152. S. Spera and A. Bax, *J. Am. Chem. Soc.*, **1991**, *113*, 5490-5492.
153. D. S. Wishart, B. D. Sykes and F. M. Richards, *J. Mol. Biol.*, **1991**, *222*, 311-333.
154. M. Kjaergaard, S. Brander and F. M. Poulsen, *J. Biomol. NMR*, **2011**, *49*, 139-149.
155. A. Chatterjee, A. Kumar, J. Chugh, S. Srivastava, N. S. Bhavesh and R. V. Hosur, *J. Chem. Sci. (Bangalore, India)*, **2005**, *117*, 3-21.
156. M. Kjaergaard and F. M. Poulsen, *J. Biomol. NMR*, **2011**, *50*, 157-165.
157. J. A. Marsh, V. K. Singh, Z. Jia and J. D. Forman-Kay, *Protein Sci.*, **2006**, *15*, 2795-2804.
158. H. Zhang, S. Neal and D. S. Wishart, *J. Biomol. NMR*, **2003**, *25*, 173-195.
159. R. E. Stafford, T. Fanni and E. A. Dennis, *Biochemistry*, **1989**, *28*, 5113-5120.
160. D. Z. Liu, E. L. LeCluyse and D. R. Thakker, *J. Pharm. Sci.*, **1999**, *88*, 1161-1168.
161. G. Manzo, M. Carboni, A. C. Rinaldi, M. Casu and M. A. Scorciapino, *Magn. Reson. Chem.*, **2013**, *51*, 176-183.
162. J. Reed and T. A. Reed, *Anal. Biochem.*, **1997**, *254*, 36-40.
163. D. Chandler, *Nature*, **2005**, *437*, 640-647.
164. A. Velazquez-Campoy, S. A. Leavitt and E. Freire, *Protein-Protein Interactions: Methods and Applications*, **2015**, 183-204.
165. M. Cho and R. D. Cummings, *Biochemistry*, **1996**, *35*, 13081-13088.
166. J. E. Ladbury, G. Klebe and E. Freire, *Nat. Rev. Drug Discovery*, **2010**, *9*, 23-27.